# LAMINAR BOUNDARY LAYER STABILITY ON A HEATED, UNDERWATER BODY

G. C. Lauchle and G. B. Gurney



Technical Memorandum
File No. TM 83-157
9 September 1983
Contract N00024-79-C-6043

Copy No. 2



The Pennsylvania State University
Intercollege Research Programs and Facilities
APPLIED RESEARCH LABORATORY
Post Office Box 30
State College, PA 16801

Approved for Public Release
Distribution Unlimited

NAVY DEPARTMENT

NAVAL SEA SYSTEMS COMMAND

UNCLASSIFIED

SECURITY CLASSIFICATION OF THIS PAGE (When Data Entered)

## REPORT DOCUMENTATION PAGE

READ INSTRUCTIONS BEFORE COMPLETING FORM

| | |
|---|---|
| 1. REPORT NUMBER: TM 83-157 | 2. GOVT ACCESSION NO. |
| 3. RECIPIENT'S CATALOG NUMBER | |
| 4. TITLE (and Subtitle): LAMINAR BOUNDARY LAYER STABILITY ON A HEATED, UNDERWATER BODY | 5. TYPE OF REPORT & PERIOD COVERED: Technical Memorandum |
| | 6. PERFORMING ORG. REPORT NUMBER |
| 7. AUTHOR(s): G. C. Lauchle and G. B. Gurney | 8. CONTRACT OR GRANT NUMBER(s): N00024-79-C-6043 |
| 9. PERFORMING ORGANIZATION NAME AND ADDRESS: Applied Research Laboratory, Post Office Box 30, State College, PA 16801 | 10. PROGRAM ELEMENT, PROJECT, TASK AREA & WORK UNIT NUMBERS |
| 11. CONTROLLING OFFICE NAME AND ADDRESS: Naval Sea Systems Command, Code NSEA-63R31, Washington, DC 20362 | 12. REPORT DATE: 9 September 1983 |
| | 13. NUMBER OF PAGES: 57 |
| 14. MONITORING AGENCY NAME & ADDRESS (if different from Controlling Office) | 15. SECURITY CLASS. (of this report): Unclassified |
| | 15a. DECLASSIFICATION DOWNGRADING SCHEDULE |

16. DISTRIBUTION STATEMENT (of this Report)

Approved for public release. Distribution unlimited.
Per NAVSEA- October 19, 1983.

17. DISTRIBUTION STATEMENT (of the abstract entered in Block 20, if different from Report)

18. SUPPLEMENTARY NOTES

19. KEY WORDS (Continue on reverse side if necessary and identify by block number)

laminar, boundary layer, heated, underwater, body

20. ABSTRACT (Continue on reverse side if necessary and identify by block number)

A large (3.05m long × 0.32m diameter) heated-surface, axisymmetric body, designed for transition research in a 1.22m diameter water tunnel is described. Boundary layer transition data are presented as functions of the heating power supplied to the body and the total concentration of free-stream particulate matter in the water. Body surface temperatures range from 0 to 25°C over the ambient water temperature, and the total heat supplied ranges from 0 to 93.3 kW. Transition arc length Reynolds

DD FORM 1 JAN 73 1473 EDITION OF 1 NOV 65 IS OBSOLETE

UNCLASSIFIED

SECURITY CLASSIFICATION OF THIS PAGE (When Data Entered)

numbers are found to vary from 4.5 million for the body operating cold to 36.4 million for the maximum heat level considered. The concentration of free-stream particles is shown to affect transition Reynolds number. These particles range in diameter from 10 to 70 μm and their concentration ranges from less than 5 to 198 particles per $cm^3$. The decrease in transition Reynolds number due to the higher concentration of particles is of order 30 percent.



Subject: Laminar Boundary Layer Stability on a Heated, Underwater Body

References: See Page 30

Abstract: A large (3.05m long × 0.32m diameter) heated-surface, axisymmetric body, designed for transition research in a 1.22m diameter water tunnel is described. Boundary layer transition data are presented as functions of the heating power supplied to the body and the total concentration of free-stream particulate matter in the water. Body surface temperatures range from 0 to 25°C over the ambient water temperature, and the total heat supplied ranges from 0 to 93.3 kW. Transition arc length Reynolds numbers are found to vary from 4.5 million for the body operating cold to 36.4 million for the maximum heat level considered. The concentration of free-stream particles is shown to affect transition Reynolds number. These particles range in diameter from 10 to 70 μm and their concentration ranges from less than 5 to 198 particles per $cm^3$. The decrease in transition Reynolds number due to the higher concentration of particles is of order 30 percent.

Acknowledgments: This work has been supported by the Applied Research Laboratory of The Pennsylvania State University under contract with the U.S. Naval Sea Systems Command, Code 63R-31. The staff of the Garfield Thomas Water Tunnel is acknowledged for help in performing this research program. Particular appreciation is extended to B. R. Parkin, S. Deutsch, F. H. Riedinger, G. D. Henderson, M. L. Billet, D. R. Stinebring and W. R. Hall.

TABLE OF CONTENTS

## LIST OF FIGURES

Figure 17. Variation of the empirical constant, $\alpha$, of Equation (9) with $Q_T$.

Figure 18. Variation of transition Reynolds number with concentration level of free-stream particles.

Figure 19. Variation of transition Reynolds number with total heating power supplied to the body.

## 1. INTRODUCTION

Early wind tunnel experiments such as those of Frick and McCullough (1942) and Liepmann and Fila (1947) suggest that the transition location of a flat plate boundary layer in air is moved forward as a result of surface heating. Because this effect is suspected to be due to the variation of fluid viscosity with temperature, it has long been speculated that the opposite effect would occur in water. In particular, the viscosity of water decreases with increasing temperature which results in a viscosity gradient close to a heated wall. The lower viscosity near the wall would tend to promote larger velocities near the wall which results in a fuller, more stable laminar velocity profile than the Blasius profile. Cooling in water (and heating in air) results in higher viscosity near the wall which can lead to an inflected velocity profile, which is unstable.

Numerical calculations by Wazzan, Okamura, and Smith (1968, 1970) confirm that wall heating can produce large increases in the transition Reynolds number of water boundary layers. In this analysis, the stability characteristics of the boundary layer is predicted from the solution of a modified, fourth-order Orr-Sommerfeld equation. Lowell and Reshotko (1974) refined these predictions further by introducing a coupled sixth-order system of vorticity and energy disturbance equations. Such calculations have demonstrated that transition Reynolds numbers (based of free-stream velocity and distance from the leading edge of a flat plate) can reach as high as 200 million for wall temperatures that are 40°C above the water temperature. These analytical methods and others are thoroughly reviewed by Reshotko (1976).

From a practical point of view, the delaying of transition can result in significant drag reduction. Reshotko (1978) presents a series of calculations of skin friction reductions for a heated flat plate at zero incidence. These calculations account for the effectiveness of transmitting the reject heat from a propulsion system to the water in the desired manner. Even with a moderately efficient heat exchanger, drag reductions in excess of 60 percent are possible at transition Reynolds numbers of the order of 70 million.

The potential payoff in drag reduction has triggered a fair amount of recent experimental research in heated laminar boundary layer flows. Strazisar, Reshotko, and Prahl (1977) present experimental results for the stability of an artificially excited laminar layer over a heated flat plate at zero incidence. For low wall overheats ($\Delta T = T_w - T_o \simeq 2.8°C$, where $T_w$ = wall temperature and $T_o$ = water temperature), they establish neutral stability curves from which critical Reynolds numbers can be determined. The results are in reasonable agreement with predictions. This work represents one of the first verifications of the predictions of Wazzan, et al (1968) and Lowell and Reshotko (1974).

The experiments of Strazisar, et al (1977) are limited to very low streamwise Reynolds numbers and overheats. Barker and Gile (1981) describe a series of heated pipe experiments of which one of the goals is to explore the upper limits of transition Reynolds number through wall heating. Their experiments are conducted on the inside of a long (6.1m), electrically heated pipe. Because the displacement thickness is thin relative to the pipe radius, the boundary layer development is approximately the same as that of a zero-pressure gradient flat plate. For a wall overheat of 8°C, Barker and Gile measure a transition Reynolds number of 47 million. As the wall heating is

increased further, these authors note that there is no further improvement in transition Reynolds number, which is in contradiction with theory. Barker and Gile attribute the observed limitations to flow asymmetries and free-stream particulates. The flow asymmetries originate in the entrance region of the pipe and are in the form of a large longitudinal vortex pair. Yao (1977) analyzes this flow in the context of the flow tube experiments and concludes that laminar instabilities will occur at high heating levels.

The effects of free-stream particulates on transition location are not at present very well understood, particularly for the very high Reynolds numbers associated with heated laminar flow. Ladd and Hendricks (1982) have initiated a quantification of these effects through tests on a small (50 mm diameter), 9:1 fineness ratio ellipsoid in a water tunnel. Their transition Reynolds numbers vary from 3.0 to 7.5 million and the tunnel water is seeded with known concentrations of particles ranging from 12 to 133 μm in diameter. Overheats range from 0 to 15°C. At the higher transition Reynolds numbers considered, Ladd and Hendricks conclude that the 80 and 133 μm particles have a degrading effect on transition Reynolds number. They estimate a critical particle Reynolds number (based on free-stream velocity and particle diameter) to be of order 700. It is pointed out that this critical Reynolds number does depend on heating level, surface finish, particle concentration and a judgment as to where the effect is important. Based on these results, it appears that free-stream particles have a detrimental effect on transition Reynolds number, but further work is necessary to identify the mechanisms by which particles destabilize the laminar layer. Chen, Goland, and Reshotko (1979) give a qualitative analysis of particle/boundary layer interaction, but the method does involve some empiricism. The authors remark that detailed experimental efforts are needed to utilize the analysis more fully.

The present investigation addresses the stability of the laminar layer over a relatively large, heated surface underwater body. This body has been designed specifically for transition research in the Garfield Thomas 1.22m diameter Water Tunnel located at the Applied Research Laboratory on The Pennsylvania State University campus. Considerable engineering effort has been given to the design and manufacture of this body so that it can be a versatile tool for transition research. The body surface is heated electrically so that heating distributions can be changed within rather broad limits. The shape of the body is one that yields a mildly favorable pressure gradient along its length. The surface of this body is polished nickel and is typical of "best effort" polishing by a skilled craftsman.

The water tunnel in which the heated body is tested is adequate for many laminar flow experimental programs. Turbulence management includes both coarse and fine mesh honeycomb and a 9:1 contraction ratio settling section. The background noise is quite low due to excellent cavitation performance of the impeller. The important feature of this facility is its high unit Reynolds number capability. After heating of the water (48°C), unit Reynolds numbers of 34.9 million/m can be achieved at a maximum water velocity of 19.8 m/s.

The transition data reported in this paper represent baseline data for the subject body. One objective is to estimate, theoretically, heat distributions for the body based on the analysis of Eisenhuth and Hoffman (1981) that should result in a stable boundary layer. These estimates are thence compared with the experimental findings. Another objective is to show qualitatively any dependence of transition Reynolds number on the concentration of free-stream particulates that are present in the water.

## 2. EXPERIMENTAL APPARATUS

### 2.1 The 1.22m Diameter Water Tunnel

The facility used in the current heated body investigation is a closed circuit, low turbulence water tunnel which has a test section length of 4.27m and a diameter of 1.22m. A complete description of this facility is given by Lehman (1959).

The turbulence in the test section is quite low for a water tunnel of this size. The settling section contraction ratio is 9:1 and its upstream section contains a flow straightener and honeycomb. The flow straightener is a 0.61m long square mesh arrangement with a cell size of 10.16 cm. The stainless steel honeycomb is situated 0.61m downstream from the straightener, is 20.32 cm thick, and has an octagonal cell shape 0.56 cm from flat to flat. Lumley and McMahon (1967) describe the design considerations for this turbulence management system. The longitudinal-component of turbulence intensity in the test section and settling section has been measured and reported by Robbins (1978). Figure 1 shows the turbulence intensity as a function of test section velocity. The higher levels below 8 m/s are suspected of being due to laminar instability within the cores of the honeycomb. The majority of the data presented in Section 4 are for velocities greater than 8 m/s where the turbulence intensity is of order 0.1 percent and the average integral length scale is 1.25 cm. As shown by Lauchle, et al (1980), this level is sufficiently low for transition research.

A feature of the 1.22m diameter water tunnel worth noting is its degassing and filtering capability. A fluid bypass system is available which is used to pass the water through 10 um filters and de-aeration modules. The maximum flow of this system is 190 ℓ/s. The de-aeration modules are small, plastic saddle-shaped units. Many thousands of these modules are contained in a large

settling tank through which the water flows. The resulting trickle of water over the modules effectively removes dissolved and free gas. Particulate matter is removed by filters in this bypass system.

The water temperature increases with time as the facility is operated. Typically, for a test section velocity of 13 m/s, the temperature increases at a rate of 1°C per hour. Testing at constant Reynolds number can be achieved by computer/tunnel operator interaction because water temperature, velocity, and pressure data are passed to an on-line VAX computer every 10s.

The water quality can be determined at any time during the course of a test. The dissolved gas content, $\alpha_o$, is measured with a Van Slyke apparatus. This instrument is primarily used in the medical diagnosis of blood, but can also be used for water. The net output is the number of moles of dissolved gas per total number of moles, expressed in parts per million (ppm).

The free gas in the test section can be measured with a laser light scattering system developed by Davis and Billet (1983). This system measures the number of bubbles per unit volume for each of seven different resolution channels ranging from 9 to 48 μm bubble diameter.

Water purity is determined by either of two methods. The one method, developed by Billet and Gates (1981), uses optical holography to sample statistically a volume of the tunnel water. Particle size distributions covering the 10 to 70 μm mean diameter range can be determined with this system. The other method involves the passing of any selected volume of tunnel water through a Nuclepore® membrane filter. Photomicrographs of the filter are produced using a Scanning Electron Microscope (S.E.M.) located at the Materials Research Laboratory on The Pennsylvania State University campus. The photomicrograph is further scanned with the S.E.M. and a statistical

estimate of the size distribution of particles is performed. This system is capable of counting any size particle, but typically the measurements cover a 1 to 1000 μm mean diameter range.

## 2.2 The Heated Body

The body shape considered for this investigation is described mathematically by a family of modified ellipse functions. It is typical of the kind of underwater body whose transition location might be effectively delayed through use of surface heating. The equation which describes the body coordinates is given by:

$$\hat{y} = [\hat{x}(2 - \hat{x})]^{1/2} - K_n \frac{C_o \hat{x}}{2a^2} \exp \{- \hat{x}^2/2a^2 - kK_n\} + \hat{x}^2 \varepsilon_L \quad , \qquad (1)$$

where $\hat{x} = x/\ell_n$, $\ell_n$ = nose length, $\hat{y} = r_b/D_{max}/2$, $D_{max}$ = maximum diameter, $K_n = \ell_n/D_{max}$, $a = 0.3$, $C_o = 0.0303$, and $k = 0.45227$. Here, x is the axial coordinate and $r_b$ is the body radius. The parameter

$$\varepsilon_L = \frac{K_n C_o}{2a^2} \exp \{- 1/2a^2 - kK_n\} \quad . \qquad (2)$$

Equation (1) describes the shape from $x = 0$ to $x = \ell_n$ ($\ell_n = 2.44$m), where $r_b = D_{max}/2$ ($D_{max} = 0.32$m). From $x = \ell_n$ to $x = L$ (L = total length = 3.05m) the body fairs into a 0.2m diameter sting. The fairing curve is a simple arc of radius 1.29m combined with an inflection curve at the sting juncture.

Calculations and measurements of the pressure distribution over this body are given by Lauchle (1979). The computed potential flow results are repeated here in Figure 2. The calculations for the pressure coefficient, $C_p$, and pressure gradient parameter, $\beta$, account for the solid blockage that occurs on bodies operating within the confines of tunnel walls. The parameter $\beta$ is calculated in the standard way, i.e.,

$$\beta = \frac{2M}{M + \lambda + 1} \quad , \tag{3}$$

where

$$M = (x/u_e)(du_e/dx) \quad , \tag{4}$$

$$u_e = \text{edge velocity} \quad ,$$

and

$$\lambda = (2x/r_b)(dr_b/dx) \quad . \tag{5}$$

It is seen from Figure 2 that this body supports a mildly favorable pressure gradient along most of its length. The parameter $\beta$ remains relatively constant and positive, indicating that the pressure gradient is relatively constant and favorable.

Given the information contained in Figure 2, temperature and heat flux distributions can be predicted that should result in laminar flow over the body to the maximum diameter point ($\hat{x} = 1$). These calculations are performed using the method of Eisenhuth and Hoffman (1981). (Note: The numerical examples given in this reference are for this particular body.) The method makes use of similarity solutions of the boundary layer equations which include the heat transfer terms, although transverse curvature terms are

neglected. The parametric procedure permits one to estimate heat distributions based on either of two criteria. The first criterion insures the maintenance of laminar flow by the addition of just enough heat to keep the local displacement thickness Reynolds number equal to the minimum critical Reynolds number established previously by Lowell and Reshotko (1974). This heating level is referred to as the "minimum distribution". The second criterion is based on the fact that there is a peak critical Reynolds number at about 65°C overheat (Lowell and Reshotko 1974). Thus, the method provides enough heat so that the peak critical Reynolds number is always maintained. This level of heating is referred to as the "maximum distribution". Heating above this level appears to provide less enhancement of the laminar layer stability. The maximum temperature distribution is independent of velocity while the minimum distribution does change with the operating velocity. Because the local Reynolds numbers are equal to or less than a critical value, no amplification of spatial disturbances in the laminar layer would be expected. The results of these predictions will be discussed in Section 4.

The heating system for the test body is designed to provide enough heat so that a theoretical maximum heat flux distribution can be achieved with the tunnel operating at its maximum velocity of 19.8 m/s and typically high water temperature of 32.2°C. In order to provide flexibility in the setting of given heating distributions, an electric heat exchanger is used in the body. This heat exchanger consists of thirty-two (32) individually controlled axial heat zones. Figure 3 shows a cut-away view of the body construction. A typical heat zone is an aluminum ring, 7.62 cm in length and 2 cm thick. The

ring is fitted with a dense array of commerically available cartridge heaters. The array of heaters are parallel wired and the common leads are connected to the power source and controller.

Each aluminum ring, or heat zone, is machine fit to its adjacent ring. When all rings are stacked together (several internal tie rods secure the assembly) an inner body of length $\ell_n$ is formed. At first assembly, this inner body was machine finished as a unit. It was then used as a mandrel for electroforming a solid nickel outer shell. The electroformed nickel outer shell is 25.4 mm thick and 2.44m long. Its surface is machined to Equation (1) using a numerically-controlled lathe and then buffed and polished to a fine finish. Surface waviness is less than 25 μm in 10 cm and the rms value of the random surface roughness is of order 0.5 μm.

The inner rings can be removed from the nickel shell for wiring or repair. When the body is reassembled, a thermally conductive, silver impregnated grease is used between the inner body and outer shell. Register marks permit the body to be reassembled in exactly the same way it was during the electroforming process; thus, minimizing misalignment which would degrade heat transfer.

The heated nose portion of the body ($0 \leq x \leq \ell_n$) is secured to a stainless steel afterbody and sting mount. Figure 4 shows a photograph of the body as installed in the 1.22m diameter test section. The afterbody is equipped with a strain gaged force balance for total drag measurements. Because of certain unresolved problems with the balance, there will be no further discussion of drag measurements in this paper.

## 2.3 Instrumentation

The instrumentation used in the experimental program includes the equipment necessary to measure body heat flux, body temperature, transition, water quality, and operational parameters. Because the techniques for measuring water quality have been discussed in Section 2.1, no further discussion is given here.

The operational parameters include test section velocity, $u_o$, ambient pressure, $P_o$, and ambient water temperature, $T_o$. Velocity is determined from the pressure drop between the settling section and the entrance of the test section. The ambient pressure is measured at the test section entrance. These pressures are determined using Validyne AP-10 absolute and DP-15 differential pressure transducers. The water temperature is monitored in the settling section with an RTD sensor with digital output. All signals are passed through a 100 channel Data Systems multiplexer and then to a VAX digital computer system for subsequent conversion to engineering units. The multiplexer updates all readings every 10s.

As noted in Figure 3, each heat zone contains a group of thermocouples (typically four). These thermocouples are made from chromel/alumel, ANSI Type K wires. The junction is crimped using commercial nickel sleeves. The measurement junction is very close to the outside surface of the inner shell. A procedure for estimating wall temperature from measurements made at the inner/outer shell interface is discussed in Section 3. The ninety (90) body thermocouples pass from the body to a copper zone box along with a thermocouple from an Omega Model TRC-III ice point cell and then to the 100 channel multiplexer. The voltages are monitored with a H/P voltmeter and transmitted to the VAX computer. The wires are individually calibrated prior to installation, where the conversion of voltage to temperature units is

performed in the VAX computer. CRT display of the body temperature distribution is achieved in nearly real time. The accuracy of the temperature measurement system is estimated to be ± 0.5°C.

Body heat flux distributions are estimated from the ratio of the electrical power supplied to each of the thirty-two (32) heat zones to the wetted surface area of the given zone. This procedure is most valid under the conditions of forced convection when the heat flux vector is radially outward. It has been estimated (Stinebring 1977) that for the typical water velocities used, the ratio of outward heat flow to inward (toward center of body) heat flow is of order $10^3$. The electrical power of each zone is varied with custom-designed SCR-type controllers; each rated at 7.5 kW. The power can be adjusted in one (1) percent increments of the load.

A Magtrol digital power meter has been modified by General Electric Corp. to selectively monitor the power supplied to each heat zone. This device integrates the product of voltage and amperage for a period of 30s and displays the wattage digitally. The manufacturer of the power meter states the accuracy to be ± 0.25 percent of the displayed reading. For the typical power levels used in this investigation, an estimated accuracy is of order ± 6 W.

In order to maintain a high-quality surface finish, the hot-film probes used for monitoring transition are not placed in the heated portions of the body. Rather, three flush mounted films (TSI Model 1471) are spaced at 120° increments around the body at the downstream end of the last heat zone. The arc length distance, s, to the probes is 2.12m. Consequently, the transition Reynolds number is measured for a fixed distance and is varied by varying the free-stream velocity. The hot-film signals are processed using standard DISA 55M01 anemometers and DISA 55D26 signal conditioners.

Transitional flow over a fixed hot-film probe is intermittent due to the creation and convection of turbulent spots. This intermittent flow is described, statistically, by the intermittency factor, $\gamma$, and the burst formation rate, N. An indicator function, I(t), is defined as a zero-one function; it is zero if the boundary layer is laminar and it is one if the layer is turbulent. The factor $\gamma$ is the time average value of I(t), and N is a count of the average number of step changes in I(t) per unit time. An intermittency detector is used to generate I(t). Its operation is as follows: (1) The hot-film signal is high-pass filtered to eliminate very low frequency components (typically set at 50 Hz), (2) the signal is differentiated and full-wave rectified so as to enhance high-frequency turbulent fluctuations, and be representative of a fluctuating vorticity signal (Taylor's frozen vorticity assumption), (3) it is integrated with a short time constant low-pass filter in order to smooth the fluctuations within a burst, and (4) the conditioned signal then passes through a Schmidt trigger with adjustable threshold. The output of the Schmidt trigger is I(t). Figure 5 shows these steps as performed on a typical hot-film signal obtained in a transitioning boundary layer. The intermittency factor is determined by passing I(t) through an integrating voltmeter and N is established by passing I(t) through a counter that triggers only on the leading edge of the unit step functions. Both quantities are determined for record lengths of 100s or more. As explained below, the value of $\gamma$ is used to establish transition for these experiments.

## 3. EXPERIMENTAL PROCEDURES

The hot-film probes are used only for the detection of transition. Therefore, an absolute calibration is not necessary. The intermittency

detector is set up using a storage oscilloscope. The velocity is adjusted so that an approximately 50 percent intermittent signal is observed. The detector threshold voltage is adjusted until the indicator function tracks with the turbulence bursts sensed by the films. This setting is very rarely changed through the course of a test. This stability is attributed to the fact that the DC-component of the film signal is removed by high-pass filtering.

Transition Reynolds number is determined from measurements of $\gamma$ vs. $u_o$. The velocity is set at a low value where $\gamma \approx 0$ (fully laminar flow over the hot film probe). It is then increased incrementally and fixed while $\gamma$ and N are established. After the higher velocities (where $\gamma = 1$) have been achieved, the sequence is repeated by decreasing $u_o$ in increments. The values of $\gamma$ and N are also determined during the decreasing velocity part of the run. It is again noted that 100s (or more) of integration time is used for each datum. The abscissa is converted to arc length Reynolds number ($Re_s = u_o s/\nu$, where $\nu$ is the kinematic viscosity determined for the water temperature at the time the datum is measured, and s = 2.12m). The arc length Reynolds number at the point where $\gamma$ = 50 percent is defined as the transition Reynolds number. These numbers may be multiplied by 1.085 to obtain the arc length Reynolds number based on edge velocity, $u_e$. This constant arises from the value of $C_p$ at s = 2.12m.

The heat flux distributions are measured in a straightforward manner. As previously noted, the electrical power supplied to a given heat zone is simply divided by the wetted surface area of the zone. The procedure is approximate because of the small, unknown amount of heat that leaks axially from zone to zone. No attempt has been made to account for this effect.

The surface, or wall temperature, $T_w$, is estimated from the measured temperature, $T_m$, by an elementary method. Figure 6 shows a cross section of the body in a plane containing a thermocouple. If $\dot{q}$ is the heat flux for the particular zone, and $\ell$ is the axial length of the zone,

$$T_w = T_m - \frac{\dot{q}}{2\pi\ell} [\ell n(r_2/r_m)/k_{AL} + \ell n(r_w/r_2)/k_{NI}] \quad . \qquad (6)$$

The constants $k_{AL}$ and $k_{NI}$ are the thermal conductivities of aluminum and nickel, respectively. Equation (6) assumes a perfect contact at the aluminum/nickel interface and that the heat flux is predominantly radially outward.

Free bubble distributions are measured with the light scattering nucleii counter of Davis and Billet (1983). These measurements are performed in the test section near the maximum diameter point of the body. Because bubble diameter is affected by dynamic pressure, these distributions are measured over a range of velocities. The tunnel pressure, $P_o$, has been held constant at 241.3 kPa (absolute) for all data presented in this paper.

The water samples used in determining particulate distributions are collected through a valve located on the bottom side of the settling section. Lauchle and Crust (1980) report that the measured distributions depend very little on free-stream velocity or pressure.

## 4. RESULTS

### 4.1 Heat Distributions

The heat distributions selected for experimental study are those minimum distributions calculated for $u_o$ = 3.05, 7.62, 12.19, and 16.76 m/s at a water temperature, $T_o$, of 25.6°C. As noted earlier, each of these distributions

should provide enough heat to keep the boundary layer neutrally stable to the point of maximum diameter on the body at velocities less than or equal to the value quoted. The heat flux distributions are shown in Figure 7 while the corresponding temperature distributions are given in Figure 8. Integration of the heat flux distribution over the wetted surface area of the body gives the total heating power supplied to the body. These integrated values are denoted by $Q_T$ and are indicated on Figures 7 and 8. In later discussions of the transition data, $Q_T$ will be used as the parameter that identifies which distribution is being referred to. It is seen from Figure 7 that the measured heat flux distributions agree well with the theoretical distributions.

The agreement between the measured wall temperature and that predicted is fair (Figure 8). The temperature data shown are measured at the value of $u_o$ noted and under laminar flow conditions. These data include the correction for skin thickness described by Equation (6), in which measured values of $\dot{q}$ are used. The scatter in these data is attributable to the slight scatter in the heat flux distributions and to the non-perfect contact between the inner and outer shells of the body.

Temperature data are not shown for the two highest heating conditions because the boundary layer was observed to be intermittent at the hot-film location. This intermittency greatly affects the heat transfer characteristics of the body and results in random fluctuations of the wall temperature. Repeatable data could not be produced near the end of the body where the layer is intermittent. Although not explored in detail, the thermocouple data can be used to indicate transition location. However, the axial resolution is poor when the intermittent flow regimes that precede fully-developed turbulent flow are large.

4.2 Water Quality

One of the objectives of this study is to establish a potential correlation between the amount of entrained particulate matter in the water and the transition Reynolds number of the body under various levels of surface heating. An effective way of doing this is to start out with relatively dirty water and then obtain transition data at selected intervals during a filtering process. The tunnel water (400 $m^3$ total volume) is drained and replaced with fresh water from a local well. This water is traditionally high in particulate matter and dissolved gas. Through use of the tunnel bypass system, the particles and dissolved gas are removed, but the process requires several hours to significantly reduce the levels. Furthermore, the bypass operation can be stopped at any time and the facility operated in its routine manner while transition data are collected.

A history of the water quality, as measured in this program, is given in Figure 9. Here, total concentration is defined as the total number of particles or bubbles measured without regard to size, per unit volume. Open circles denote those particles measured using the holographic technique and the solid circles represent additional data acquired using the S.E.M. technique. Triangles are used to denote the free gas bubbles measured with the light scattering method. The mean diameter of the particles and bubbles is also shown in Figure 9 as a function of the filtering time. Transition data are obtained for each condition indicated by a datum point on this figure. It is emphasized that a given condition was maintained for as long a period as necessary in order to acquire the transition data.

The purest water considered occurs after several hours of filtering. The concentration of bubbles and particles are nearly equal at this condition, but very low; less than $10/cm^3$. Prior to this condition, Figure 9 shows

that the water is dominated by particles, typically 20 to 26 μm in diameter.

Measured particle and bubble distributions are shown in Figure 10. The cross-banded area of this figure represents the spread of typical particulate distributions measured in various oceans (Barker and Gile 1981). From this figure it is seen that the water tunnel distributions considered fall below and within those of typical ocean water. Error bands are indicated for the bubble distributions because these measurements exhibit considerable scatter. The scatter is due to the dependence of bubble size on velocity.

### 4.3 Baseline Transition Results

In this section, transition data are presented for the purest conditions of tunnel water ($t/t_{TOTAL} \geq 0.94$) where the aggregate concentration of particles and bubbles is less than $15/cm^3$. These data are considered baseline data and represent the best performance of the body. It is noted that the body was installed in the tunnel four different times during a 12 month time period, and that these baseline transition data were repeatable to within 5 percent. The data presented are for one hot-film probe only because two of the three probes installed in the body did not perform satisfactorily.

Figures 11 through 14 show the baseline transition region statistical quantities $\gamma$ and $N$ as functions of the arc length Reynolds number. The transition Reynolds number is identified at $\gamma = 50$ percent. The intermittency and burst rate distributions are seen to broaden as the heating level (and transition Reynolds number) increases. Within the experimental scatter, no dependence of $\gamma$ (or $N$) on whether $u_0$ is increasing or decreasing is observed. A hysteresis might be expected, however, if the integration time were decreased and the rate of velocity change increased. Such data could no

longer be classed as steady state, but as transient and would depend on the thermal inertia of the body itself.

The cold body intermittency distribution is considered to be quasi-steady. With the hot-film probe situated at a relatively large arc length distance from the nose, the velocity must be set quite low ($u_o \sim 1.5$ m/s) for laminar flow. At speeds lower than 3 m/s, the water velocity drifts thus necessitating the collection of data over shorter time intervals. Nevertheless, the cold body transition Reynolds number of 4.5 million agrees well with that measured by other methods on another body of this size and shape (Lauchle, et al 1980).

The heating distributions associated with the transition data of Figures 11 through 14 are based on predictions that require the local displacement thickness Reynolds number to be less than a critical value, $Re_{\delta^*crit}$. A given heat distribution should therefore provide enough heat to maintain full laminar flow over the body at the velocity noted for the prediction. A critical arc length Reynolds number can be defined as one based on the velocity used in the heat prediction and the arc length from the nose to the hot-film probe. A comparison of this critical Reynolds number with the measured transition Reynolds number is given in Figure 15. One would expect the critical curve to fall substantially below the transition curve, as it does for the lower values of $Q_T$. However, for $Q_T > 60$ kW, the two curves converge and cross. This behavior is not inconsistent with what Barker and Gile (1981) observed for a heated pipe flow. The theoretical methods used by Barker and Gile are analogous to those used here (Eisenhuth and Hoffman 1981). It is reasoned that for the higher Reynolds numbers (or higher heating

levels), free-stream disturbances, surface flaws, and system idiosyncrasies become more important; their presence affects the measured results, but are unaccounted for in the theoretical models.

The application of Emmons' (1951) spot theory allows one to express the burst frequency in terms of the intermittency factor. Following Gedney (1979), a line source density function is assumed, for which

$$N\Delta x/u_o \simeq 4.76\ [(1 - \gamma)\ell n(\frac{1}{1-\gamma})]^{1/2} \quad . \tag{7}$$

The streamwise extent of the transition zone is denoted by $\Delta x$. This length is not known for the present measurements, so it must be estimated. Chen and Thyson (1971) suggest that

$$Re_{\Delta x} \simeq 60 Re_t^{2/3} \quad , \tag{8}$$

where $Re_t$ is the length Reynolds number where bursts first appear. Rearrangement of Equation (7) using Equation (8), and using the fact that $Re_s \sim Re_t$ (s = distance to the measurement probe) permits one to write:

$$\frac{Ns}{Re_s^{1/3} u_o} = \alpha[(1 - \gamma)\ell n(\frac{1}{1-\gamma})]^{1/2} \quad , \tag{9}$$

where $\alpha$ is a proportionality constant.

Figure 16 shows the baseline non-dimensional burst rates as a function of intermittency factor for the four heating levels considered. The constant $\alpha$ of Equation (9) is adjusted so that the theoretical curve matches the data. This matching reveals that $\alpha$ depends on $Q_T$ in a non-linear manner, Figure 17. This dependence cannot be explained further, until additional information is obtained on the behavior of $\Delta x$ with varying levels of surface heating. (The constants in Eqs. (7) and (8) are based on experiments with unheated walls.)

4.4 Effect of Increased Particulate Level

In reference to Figure 9, the baseline transition results of Section 4.3 are for normalized filtering times greater than 0.94. In this section, transition data are presented for much shorter filtering times where the water is contaminated with high levels of particulate matter. Because the number of particles per unit volume is far greater than the number of observed bubbles, the particle concentration can be used as an independent variable.

Figure 18 shows the measured transition Reynolds numbers for the body operating at three different heating levels as a function of total particle concentration. Here, total concentration is the total number of particles measured throughout the 10 to 70 μm diameter size range per unit volume of water. Figure 18 shows that the laminar flow performance of the body degrades with increasing concentration of free-stream particulates. The effect seems to be progressively more important as the heating level increases. This is more easily seen by replotting the data as shown in Figure 19. The transition Reynolds number is decreased by as much as 30 percent due to the introduction of the higher levels of free-stream particles.

The results given in Figures 18 and 19 show that the decrease in transition Reynolds number with increasing particle concentration is a gradual dependence. This is analogous to what Klebanoff, Schubauer, and Tidstrom (1955) observed for two-dimensional roughnesses on a flat plate. The transition Reynolds number gradually decreases as the roughnesses protrude farther and farther into the boundary layer. The mechanism is explained simply. The roughness creates an inflected velocity profile which leads to wave motion in the laminar layer. For small roughnesses, these waves damp out, but as the roughness height increases, the waves are less damped and grow. The amplification of these roughness-induced

waves leads to earlier transition. It is noted that Klebanoff, et al (1955) observed a different effect for three-dimensional spherical elements that were fixed on the surface. A very pronounced change in transition Reynolds number occurs when the sphere diameter becomes approximately equal to $\delta^*$, the displacement thickness. From these three-dimensional results, an average critical sphere diameter Reynolds number (based on local velocity at the top of the sphere) of 577 is suggested. The mechanism for the abrupt change in transition Reynolds number appears in the formation of an attached turbulent wedge from the roughness element. Thus, transition of the boundary layer is caused by a direct seeding of turbulence from the wake of the attached element, rather than from the amplification of wavelike disturbances as were observed to occur for the two-dimensional elements. Hall (1967) reports similar results for spheres that are attached as well as detached from the surface.

In light of the above discussion, the current results suggest that free-stream particles that enter the boundary layer affect transition by inducing a locally inflected velocity profile. Exactly where along the body this effect becomes important cannot be established from the data obtained, but it is speculated that the particle size relative to the displacement thickness is a key parameter. Calculations of the heated, laminar boundary layer development along this body have been performed using the methods of Gentry and Wazzan (1976). For the 75.4 kW heating condition, and for a velocity of 14.6 m/s, which is approximately the observed baseline transition velocity, $\delta^*$ is calculated to be 106 μm at s = 1.92m (just upstream of the transition probe). At this station along the body, the calculation suggests that $d_{max}/\delta^* \simeq 0.66$, which may not be an insignificant value. At stations closer to the nose,

this ratio would be expected to be larger, but again, it cannot be determined where along the body a particle may actually enter the boundary layer. This is a point which possibly deserves further investigation.

As a final note, the observance of no abrupt change in transition Reynolds number with changes in particle concentration (10 μm ≤ d ≤ 70 μm) suggests that turbulent seeding from the particles does not occur in the experiments described here. Such seeding may possibly occur, however, if some of the particles actually stick to the surface. As pointed out by Talbot, et al (1980), thermophoresis considerations would make this possibility unlikely for small particles in a boundary layer over a heated surface. With no clearly defined "critical" concentration, a critical particle Reynolds number cannot be determined from the results of these experiments.

## 5. CONCLUSIONS

The present experimental investigation has shown that the transition Reynolds number can be significantly increased on a heated, underwater body. The maximum transition Reynolds number achieved is 36.4 million with an average overheat of 25°C. The total heating power for this level of performance is 93.3 kW. The maximum Reynolds number can be compared to 4.5 million for the body operating with no heat. Although higher heating levels were not considered, the results indicate that further increases in heating power would yield only marginal increases in the transition Reynolds number. For heating levels below 60 kW (average overheat 20°C), the increase in transition Reynolds number with heat agrees well with theory. Above this level, the agreement is not good. A similar trend was observed for a heated pipe flow (Barker and Gile 1981). This degradation in performance is

attributed to free-stream disturbances, surface disturbances, and system idiosyncrasies, none of which are accounted for in the theory, and none of which could be quantitatively determined in the context of these experiments.

Particles in the free stream are considered a free-stream disturbance that may lead to increased laminar instability. Their effect on transition Reynolds number has been demonstrated in these experiments. The particles considered range from 10 μm to 70 μm in diameter. At high concentrations ($\sim 200/cm^3$), these particles decrease the transition Reynolds number by as much as 30 percent at high heat levels. The degradation is less severe at lower heating levels. Because transition Reynolds number increases monotonically with heating level, an alternative interpretation is that the instabilities created by a given size range of particles becomes progressively more severe as the particle-free (baseline) transition Reynolds number increases. This is an expected trend because the ratio of particle size to laminar boundary layer thickness becomes larger at a fixed arc length as the Reynolds number increases.

The decrease in transition Reynolds number with increasing concentration of particles is a gradually decreasing function. It is difficult, therefore, to identify a critical concentration from which critical particle Reynolds numbers can be inferred. Additional work is necessary to identify these particle Reynolds numbers. The experiments are best performed at constant Reynolds number while various sizes of particles are introduced at a fixed concentration. Work is continuing in this area.

## REFERENCES

Barker, S. J. and Gile, D. 1981 J. Fluid Mech. 104, 139.

Billet, M. L. and Gates, E. M. 1981 Trans. A.S.M.E., J. Fluids Engr. 103, 8.

Chen, C. P. Goland, Y. and Reshotko, E. 1979 Generation Rate of Turbulent Patches in the Laminar Boundary Layer of a Submersible, in Viscous Flow Drag Reduction (ed. Hough, G. R.), p. 73 (Prog. in Astronautics and Aeronautics 72).

Chen, K. K. and Thyson, N. A. 1971 AIAA J. 9, 821.

Davis, R. J. and Billet, M. L. 1983 Light-Scattering System: Probe Volume Statistical Analysis, Proc. A.S.M.E. Cavitation and Multiphase Flow Forum, Houston, TX.

Eisenhuth, J. J. and Hoffman, G. H. 1981 J. Hydronautics 15, 90.

Emmons, H. W. 1951 J. Aero. Sci. 18, 490.

Frick, C. W., Jr. and McCullough, C. B. 1942 Tests of a Heated Low Drag Airfoil, NACA APR.

Gedney, C. J. 1979 Wall Pressure Fluctuations During Transition on a Flat Plate, Report No. 84618-1, MIT, Acoustics and Vibration Laboratory.

Gentry, A. E. and Wazzan, A. R. 1976 The Transition Analysis Program System Vol. II - Program Formulation and Listings, Report MDC J7255-02, McDonnel Douglas Corp.

Hall, G. R. 1967 AIAA J. 5, 1386.

Klebanoff, P. S., Shubauer, G. B. and Tidstrom, K. D. 1955 J. Aero. Sci. 22, 803.

Ladd, D. M. and Hendricks, E. W. 1982 Effects of Surface Roughness and Particulates on Heated Laminar Flow, Proc. of Appl. of Lda'sto Fluid Mech., Portugal.

Lauchle, G. C. 1979 J. Hydronautics 13, 61.

Lauchle, G. C. and Crust, J. B. 1980 Particulate Distributions in the Garfield Thomas Water 48-Inch Diameter Water Tunnel, Report TM 80-162, The Pennsylvania State University, Applied Research Laboratory.

Lauchle, G. C., Eisenhuth, J. J. and Gurney, G. B. 1980 J. Hydronautics 14, 117.

Lehman, A. F. 1959 The Garfield Thomas Water Tunnel, Rept. NOrd 16597-56, The Pennsylvania State University, Ordnance Research Laboratory.

Liepmann, H. W. and Fila, G. H. 1947 Investigations of Effects of Surface Temperature and Single Roughness Elements on Boundary Layer Transition, NACA Rept. 890.

Lowell, R. L. and Reshotko, E. 1974 Numerical Study of the Stability of a Heated Boundary Layer, Report FTAS/TR-73-95, Case Western Reserve University.

Lumley, J. L. and McMahon, J. F. 1967 Trans. A.S.M.E., J. Basic. Engr. 89, 764.

Reshotko, E. 1978 Heated Boundary Layers, Proc. 12th. Symp. on Naval Hydrodynamics, Washington, DC, p. 33.

Reshotko, E. 1976 Ann. Rev. of Fluid Mech. 8, 311.

Robbins, B. E. 1978 J. Hydronautics 12, 122.

Stinebring, D. R. 1977 (unpublished analysis).

Strazisar, A. J., Reshotko, E. and Prahl, J. M. 1977 J. Fluid Mech. 83, 225.

Talbot, L., Cheng, R. K., Schefer, R. W. and Willis, D. R. 1980 J. Fluid Mech. 101, 737.

Wazzan, A. R., Okamura, T. T. and Smith, A. M. O. 1970 The Stability and Transition of Heated and Cooled Incompressible Boundary Layers, Proc. 4th. Int. Heat Transfer Conf., Paris.

Wazzan, A. R., Okamura, T. T. and Smith, A. M. O. 1968 Trans. A.S.M.E., J. Heat Transfer 90, 109.

Yao, L-S. 1977 Entry Flow in a Heated Tube, Report R-2111-ARPA, The Rand Corporation, Santa Monica, CA.

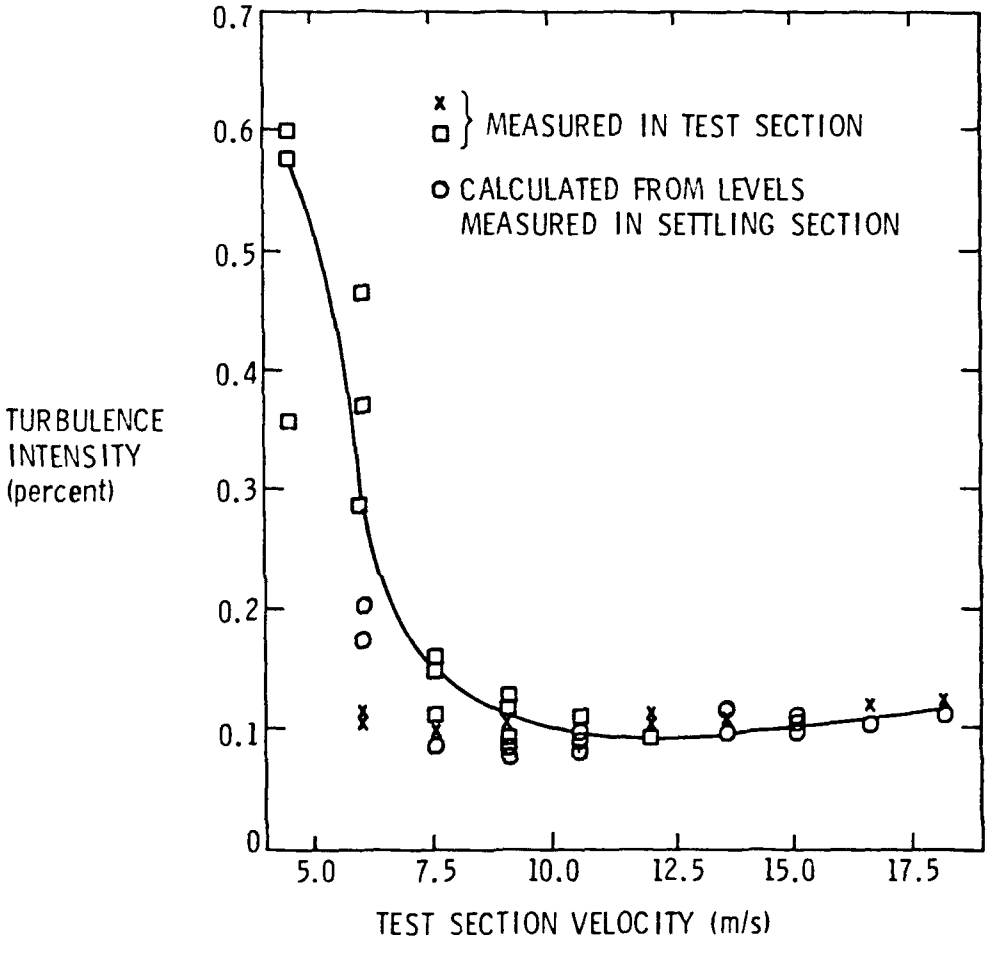


Figure 1. Test section turbulence intensity as measured in the 1.22m diameter water tunnel by Robbins (1978).

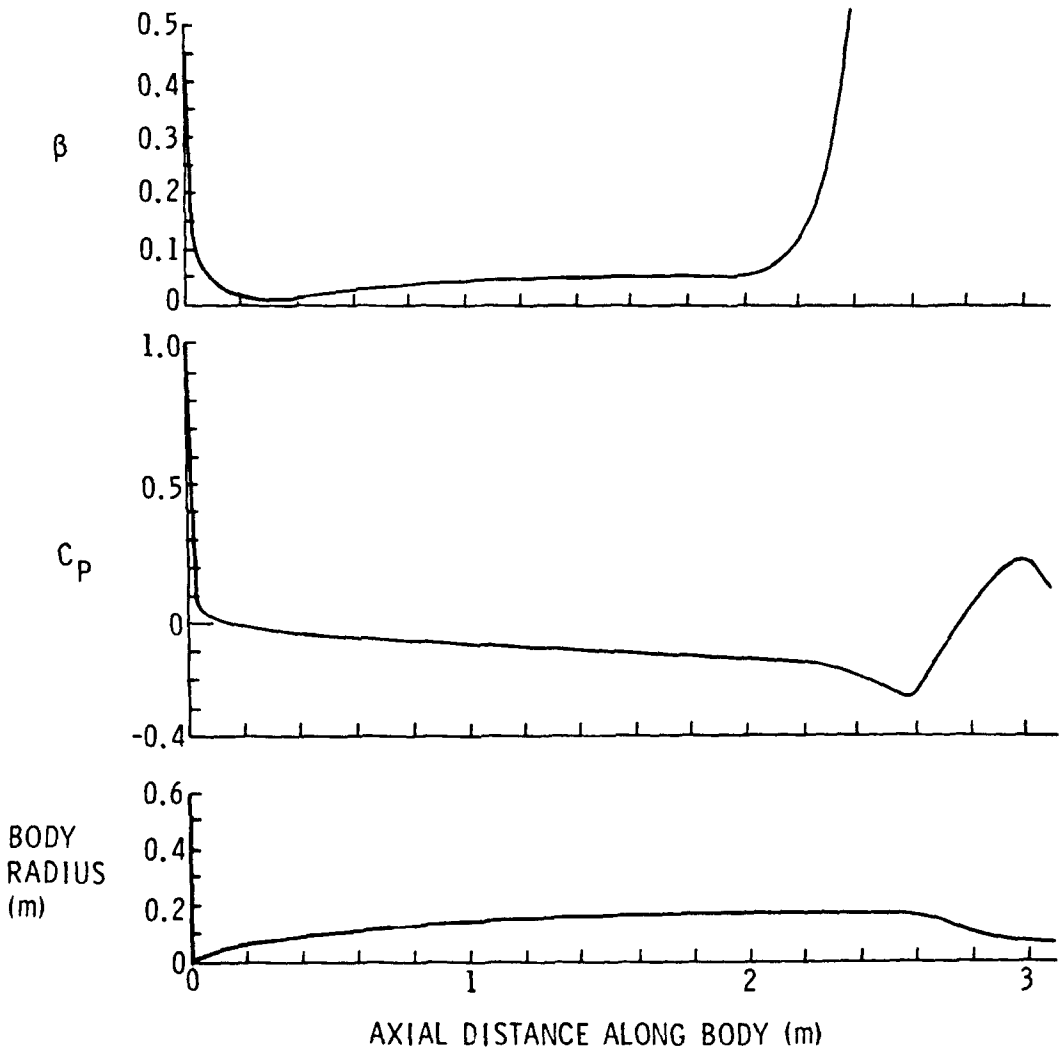


Figure 2. Potential flow calculations of pressure coefficient and pressure gradient parameter for the heated body including wall effects.

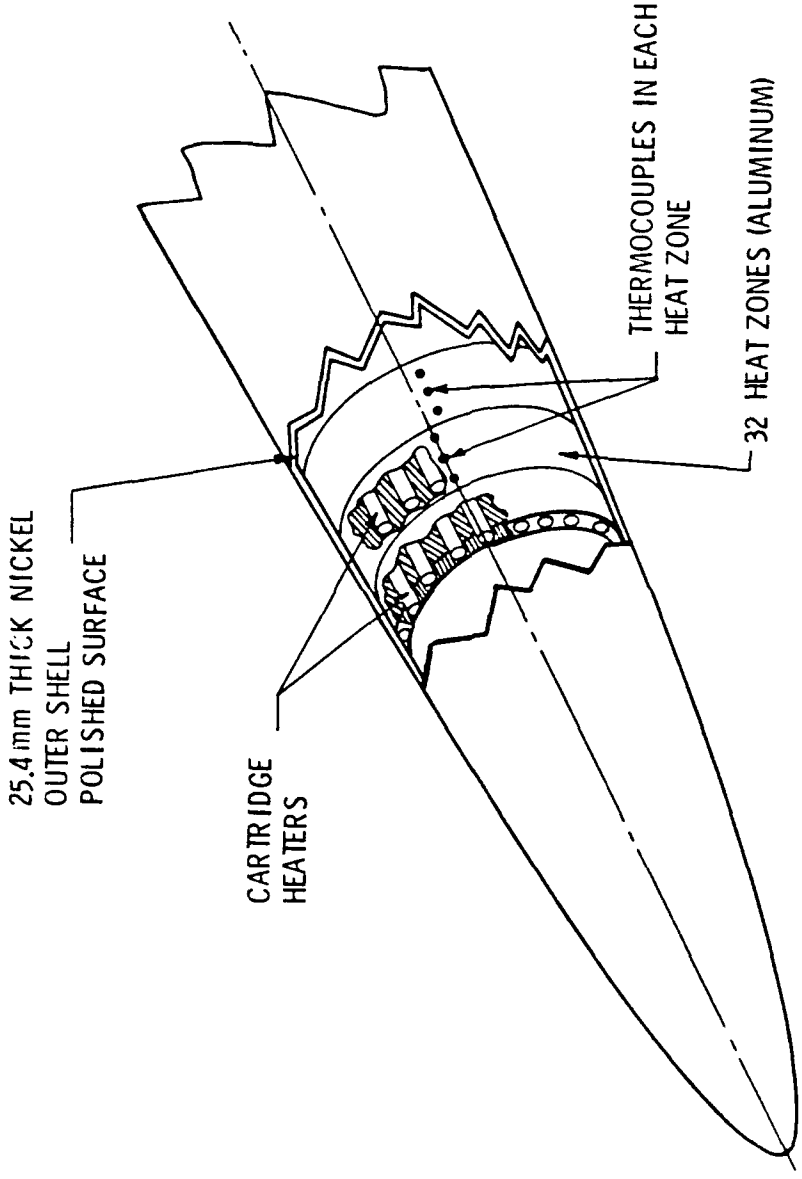


Figure 3. A schematic view of the heated body.

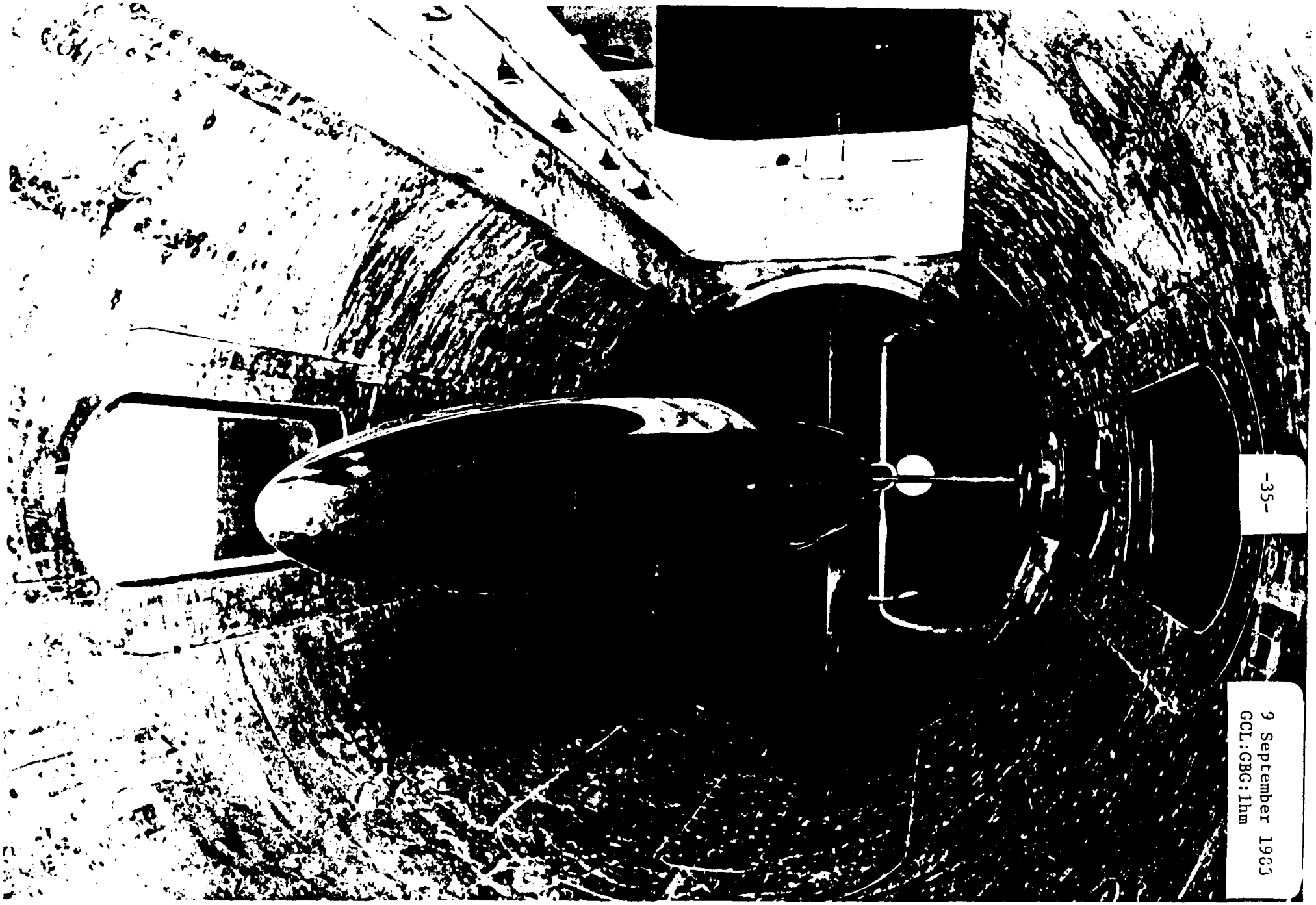


Figure 4. Photograph of the heated, laminar flow body in the 1.22m diameter test section.

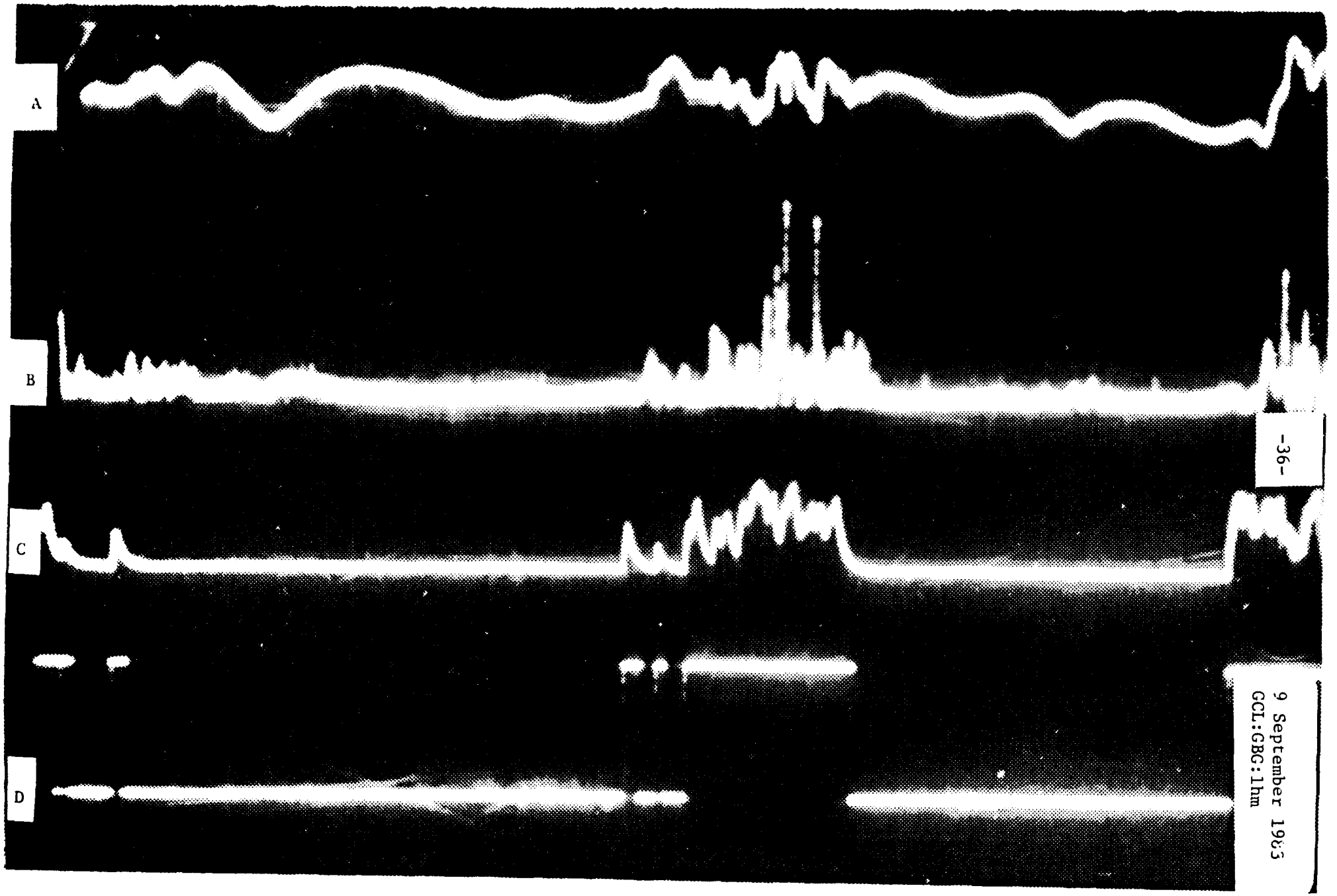


Figure 5. Oscilloscope traces showing: (a) Hot film signal, (b) Signal (a) after differentiation and full-wave rectification, (c) Signal (b) after low-pass filtering, and (d) Schmidt trigger output (indicator function) after operation on Signal (c).

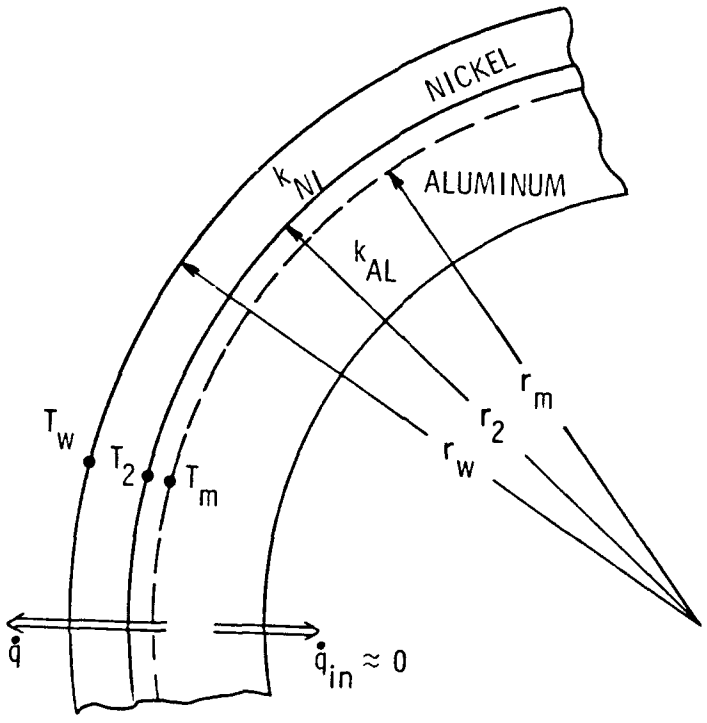


Figure 6. Definition of variables used in Equation (6).

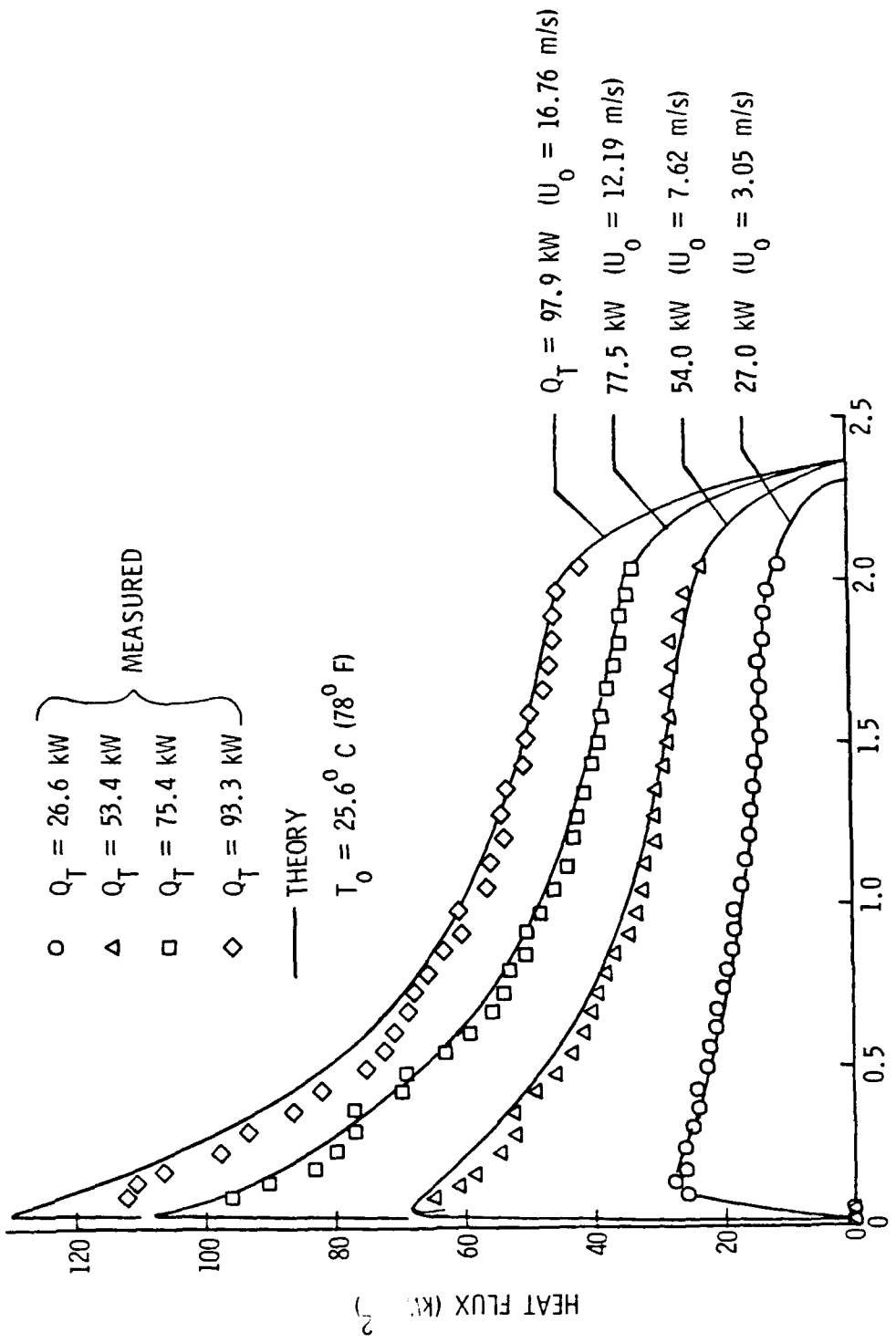


Figure 7. Predicted and measured heat flux distributions for the heated body.

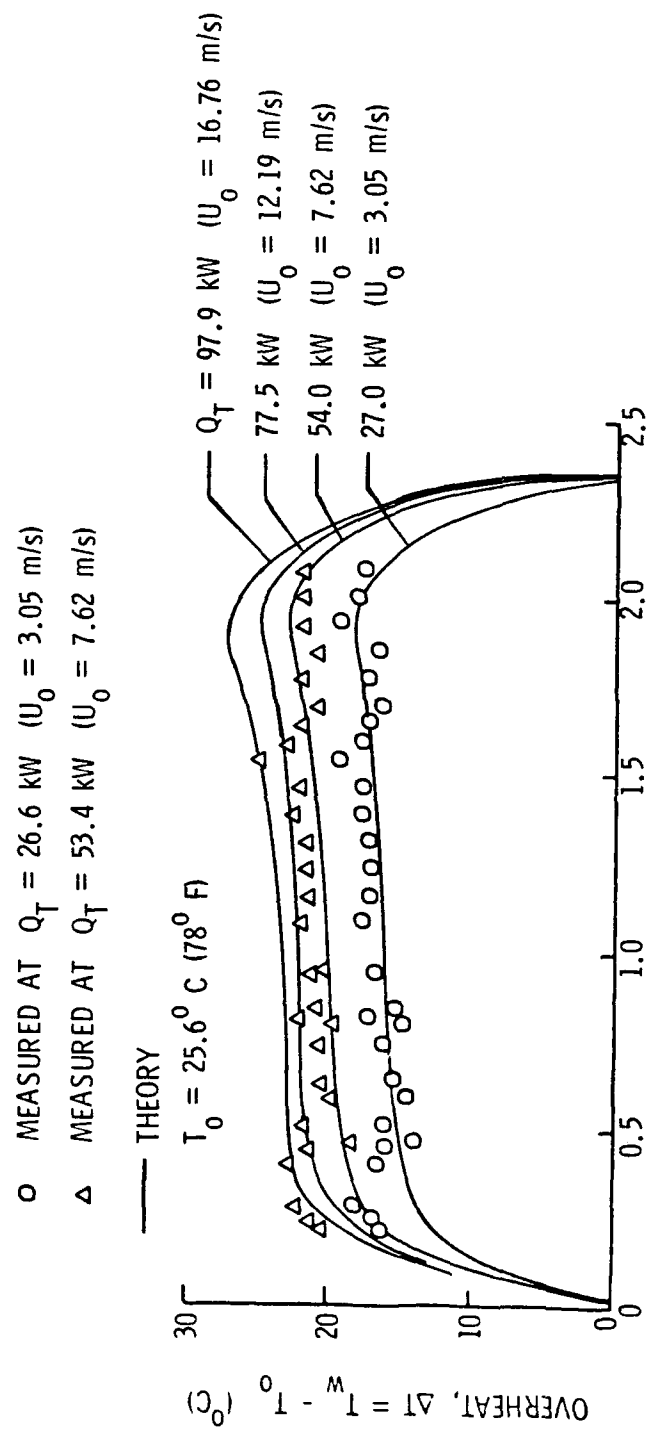


Figure 8. Predicted and measured wall temperature distributions for the heated body.

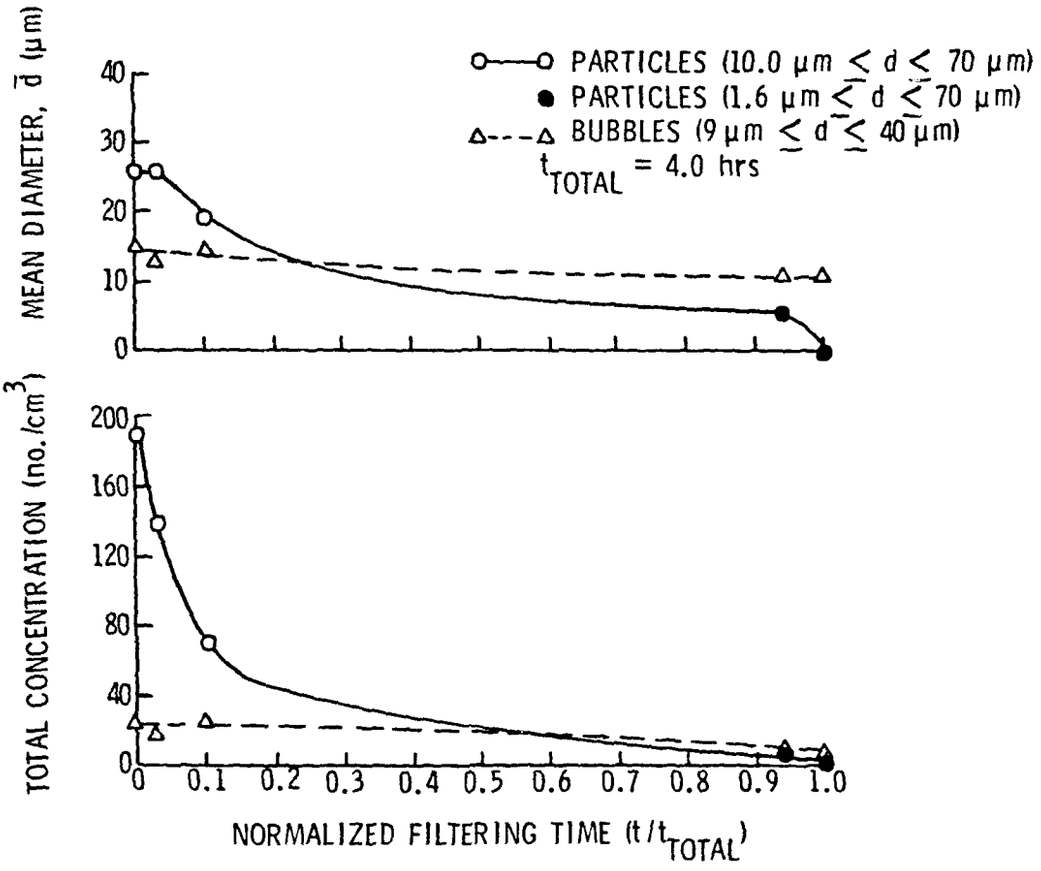


Figure 9. Variation of free-stream particulates and bubbles with bypass filtering time.

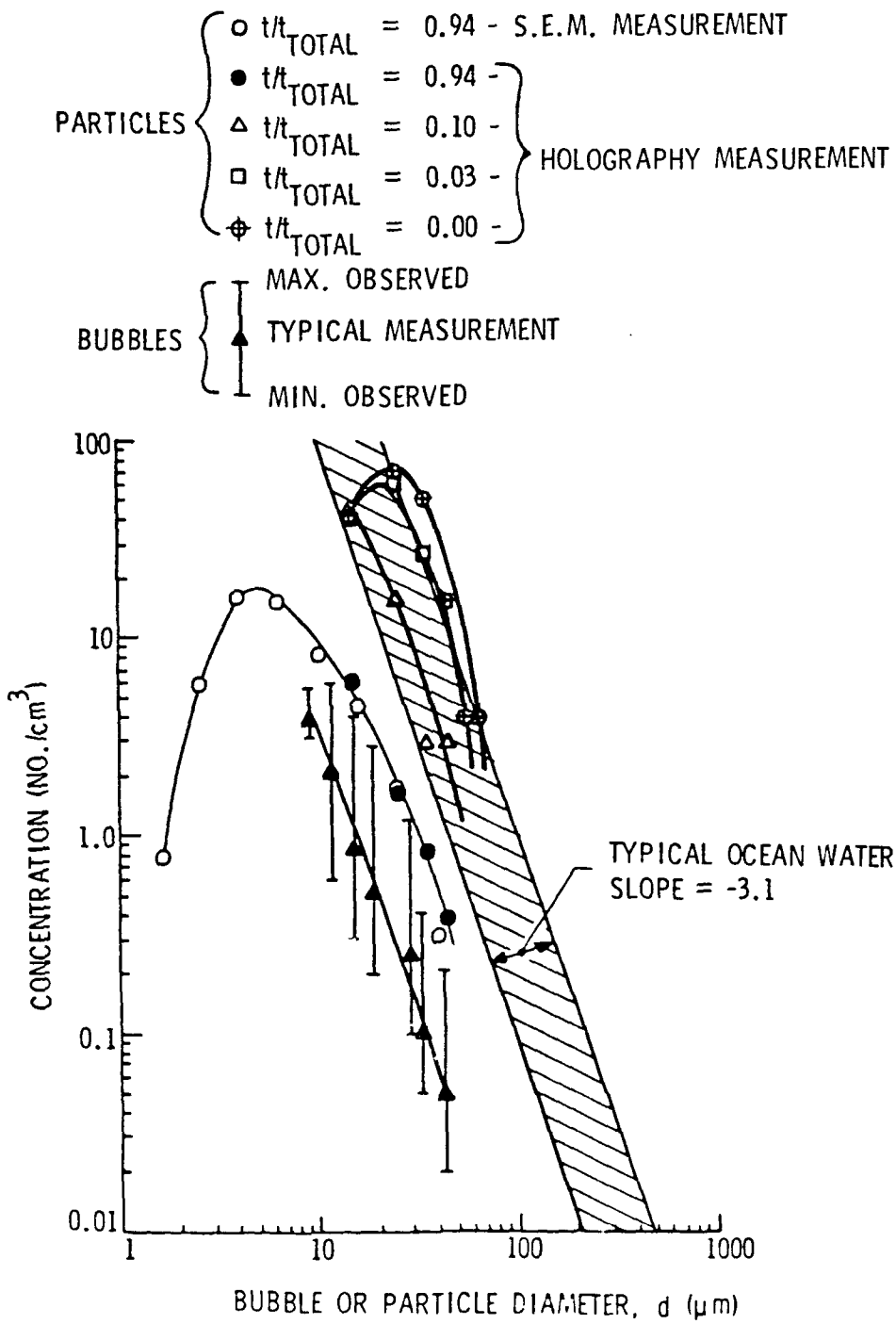


Figure 10. Particle and bubble size distributions measured during various phases of the experimental program.

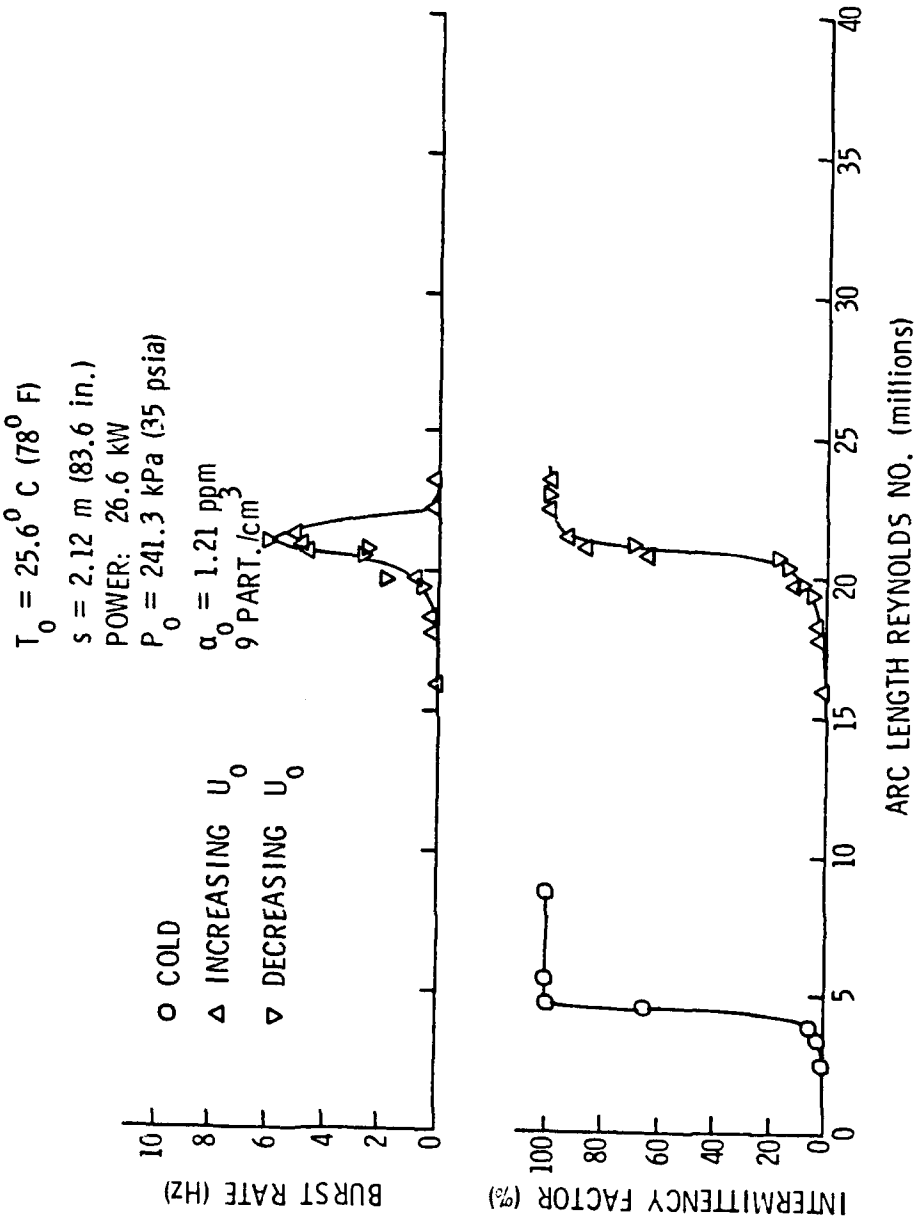


Figure 11. Variation of turbulence intermittency and burst rate with Reynolds number for baseline conditions and $Q_T$ = 26.6 kW.

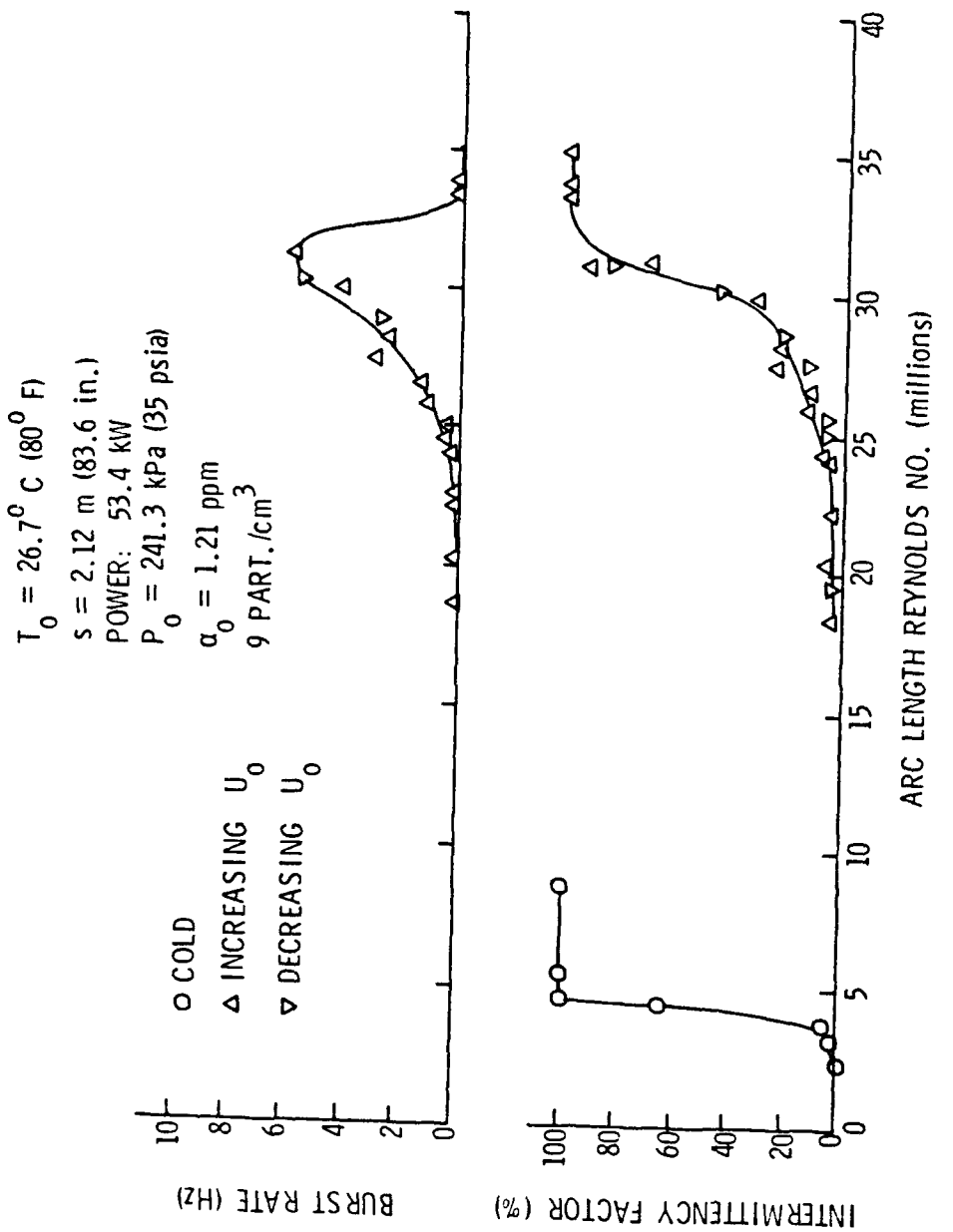


Figure 12. Variation of turbulence intermittency and burst rate with Reynolds number for baseline conditions and $Q_T$ = 53.4 kW.

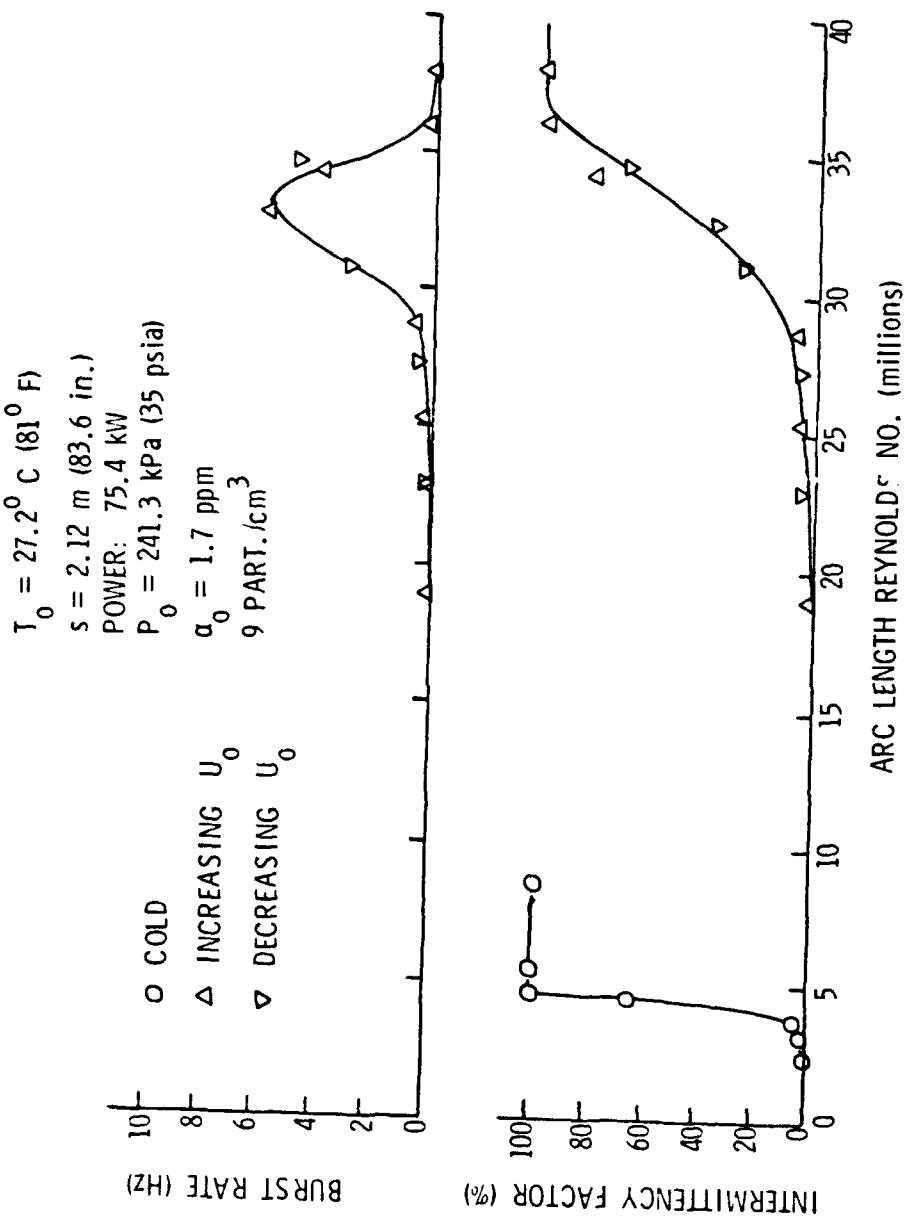


Figure 13. Variation of turbulence intermittency and burst rate with Reynolds number for baseline conditions and $Q_T$ = 75.4 kW.

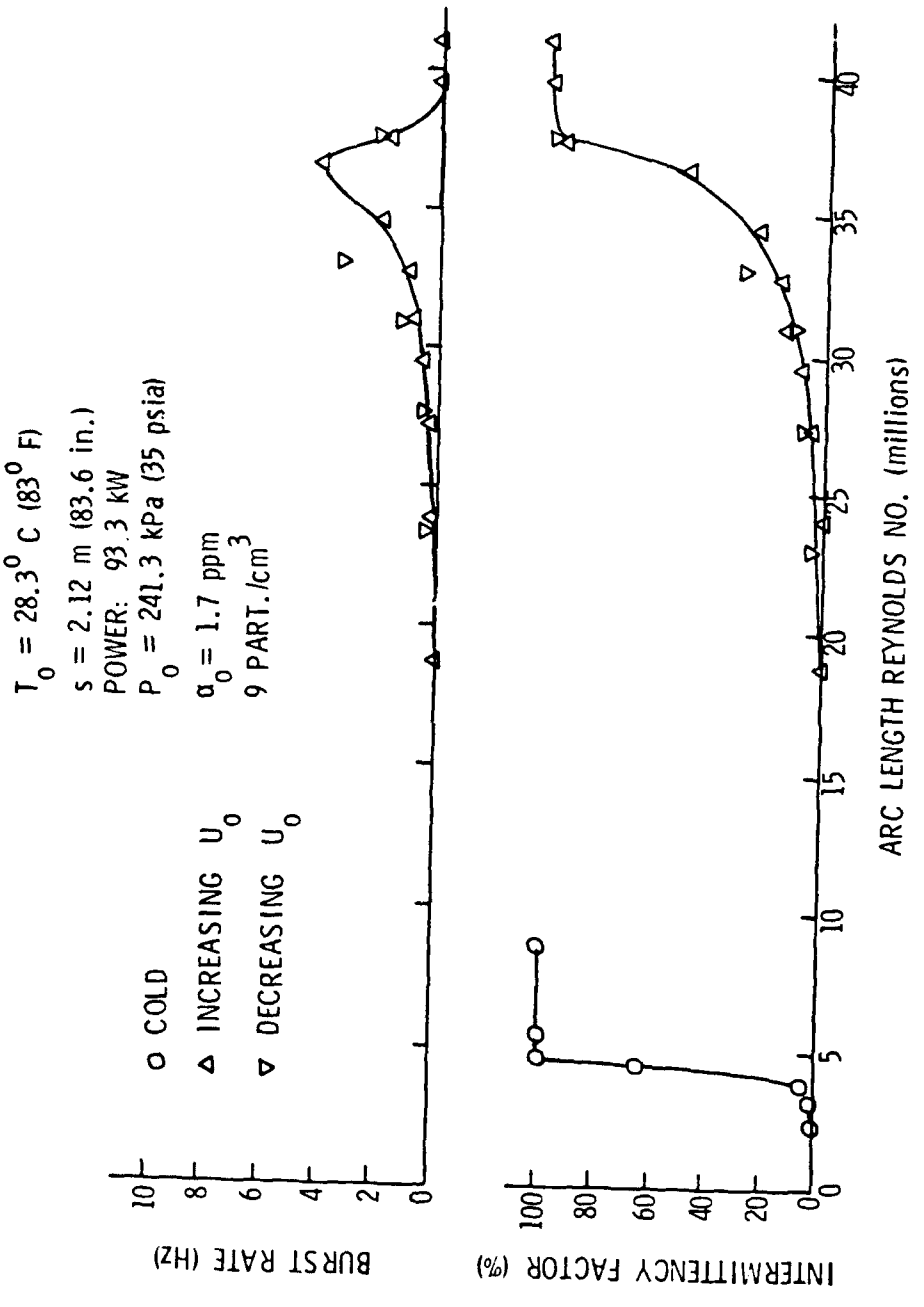


Figure 14. Variation of turbulence intermittency and burst rate with Reynolds number for baseline conditions and $Q_T$ = 93.3 kW.

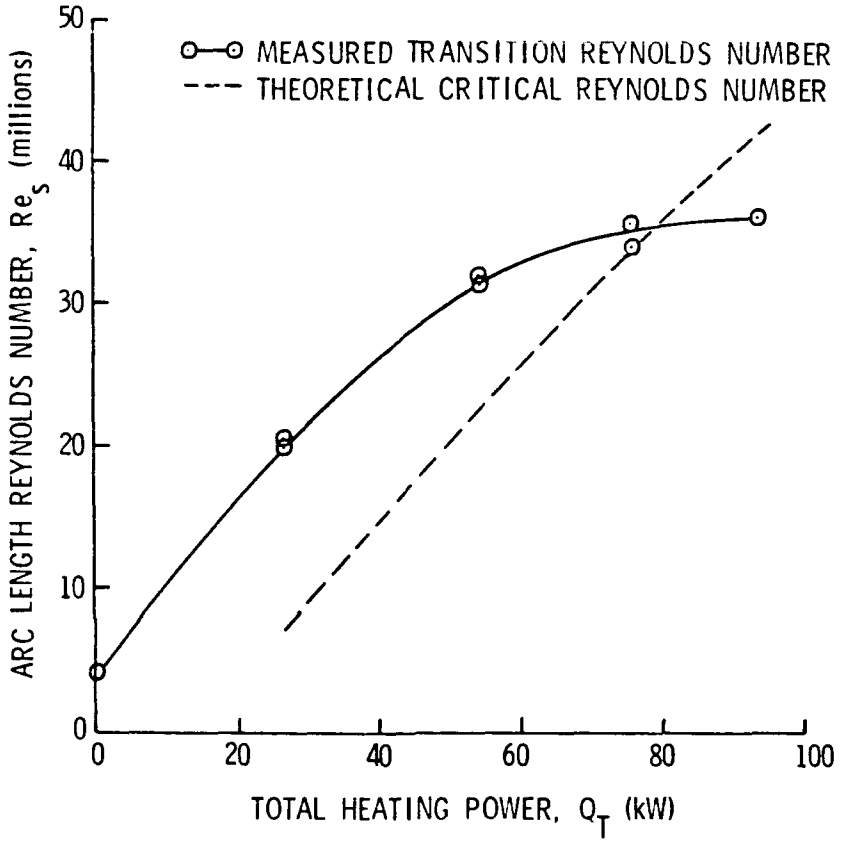


Figure 15. Comparison of experimentally determined transition Reynolds numbers with theoretical critical Reynolds numbers.

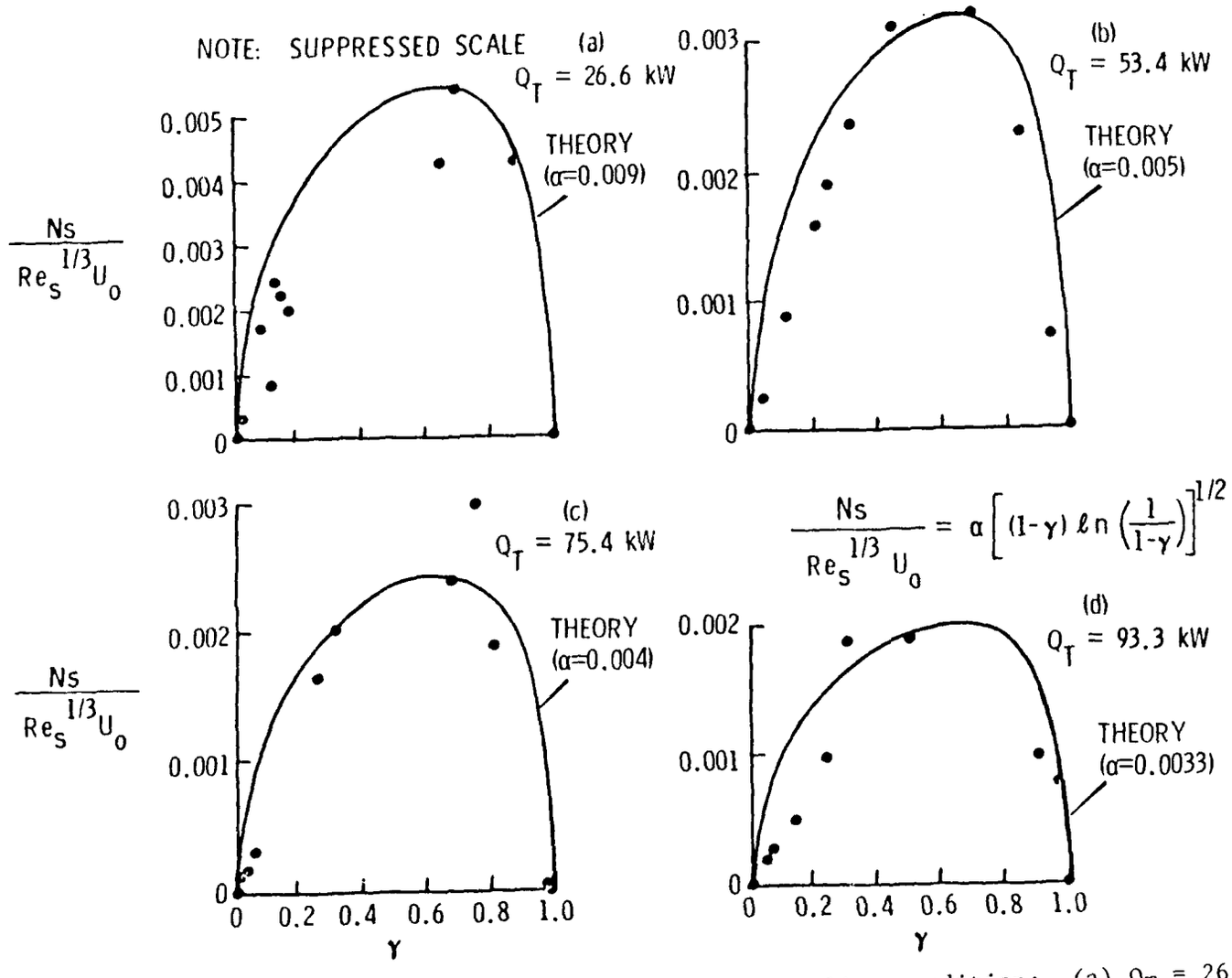


Figure 16. Non-dimensional burst rate distributions for the baseline condition: (a) $Q_T$ = 26.6 kW, (b) $Q_T$ = 53.4 kW, (c) $Q_T$ = 75.4 kW, and (d) $Q_T$ = 93.3 kW.



9 September 1983
GCL:GBG:lhm

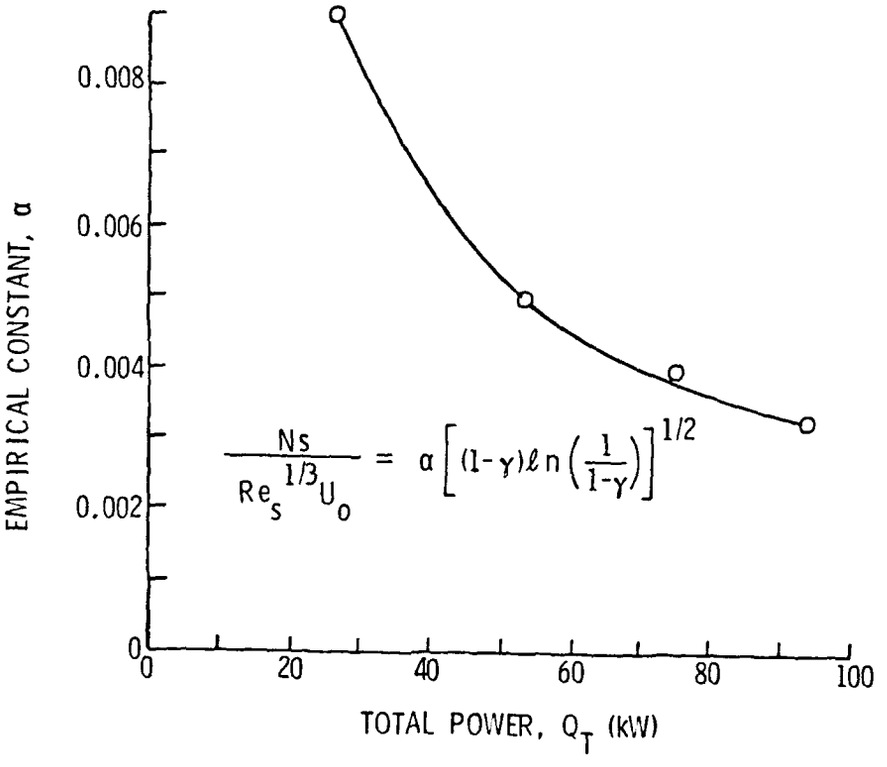


Figure 17. Variation of the empirical constant, α, of Equation (9) with $Q_T$.

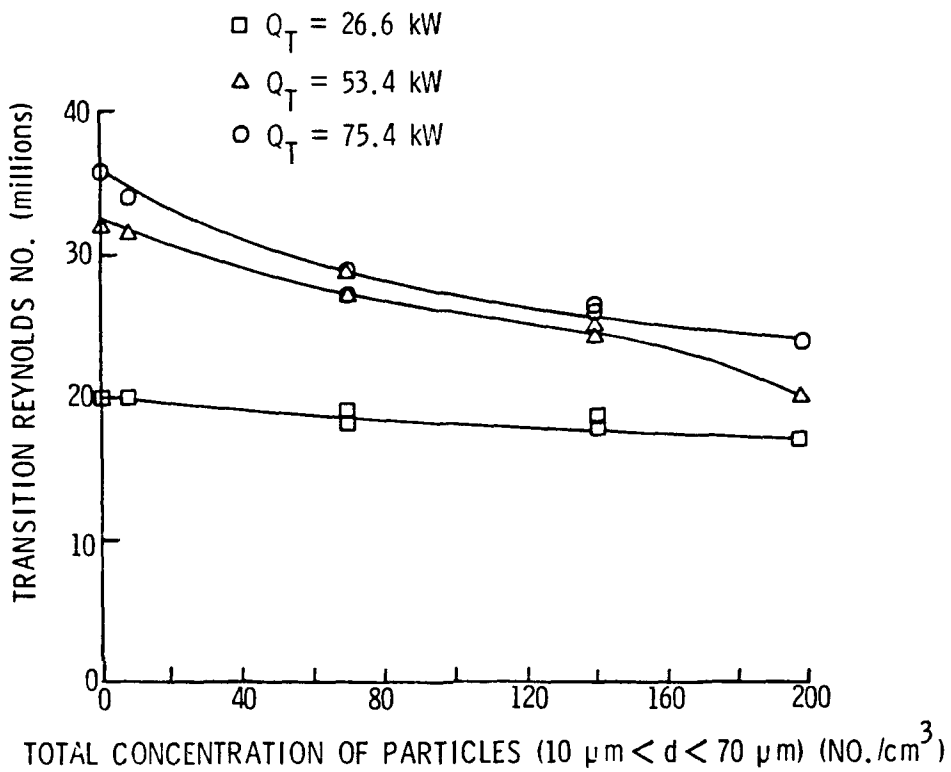


Figure 18. Variation of transition Reynolds number with concentration level of free-stream particles.

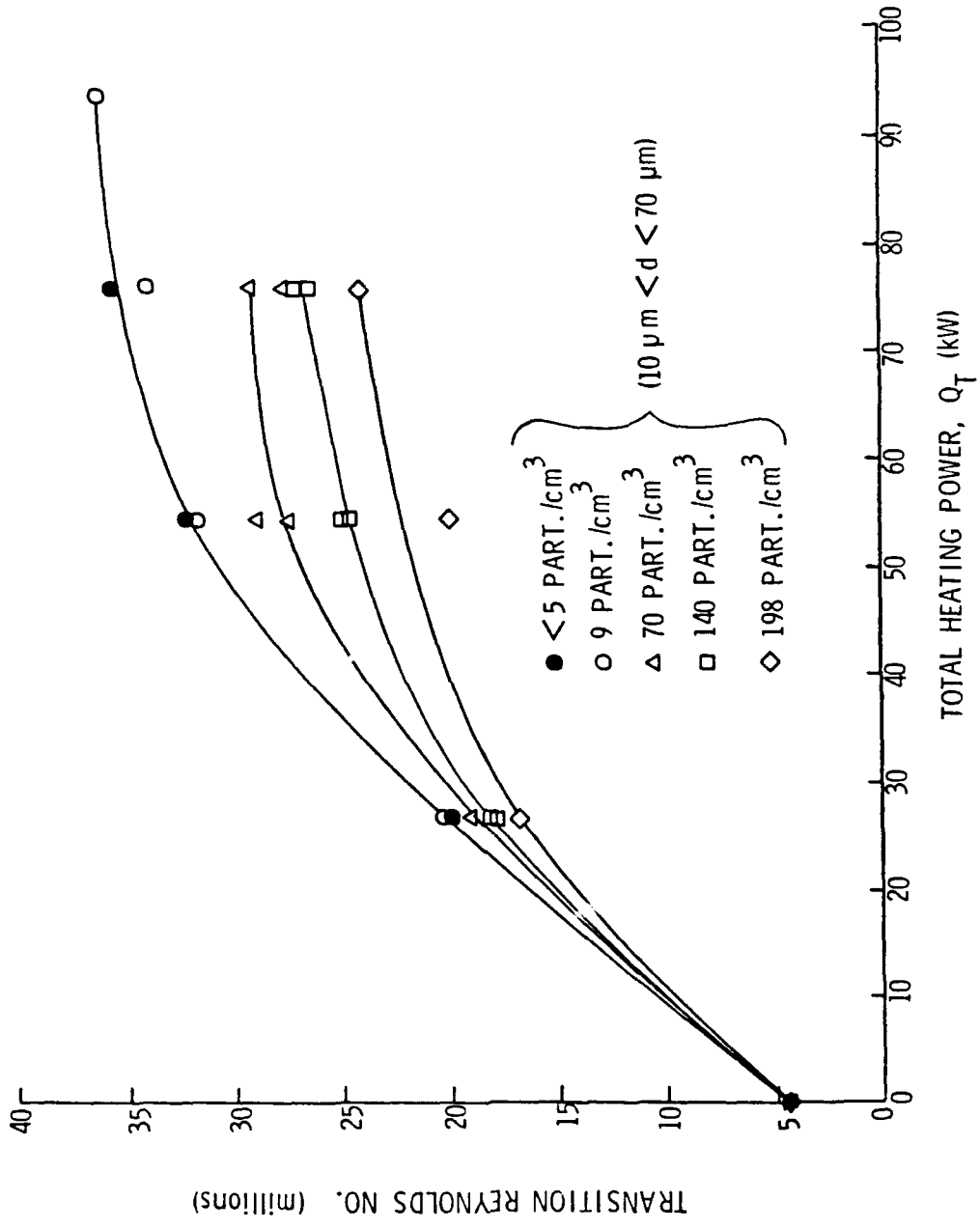


Figure 19. Variation of transition Reynolds number with total heating power supplied to the body.

DISTRIBUTION LIST FOR UNCLASSIFIED TECHNICAL MEMORANDUM FILE NO. 83-157,
by G. C. Lauchle and G. B. Gurney, dated 9 September 1983

Commander
Naval Sea Systems Command
Department of the Navy
Washington, DC 20362
Attn: Library
Code NSEA-09G32
(Copies 1 and 2)

Commander
Naval Sea Systems Command
Department of the Navy
Washington, DC 20362
Attn: R. Keane
Code NSEA-3213
(Copy No. 3)

Commander
Naval Sea Systems Command
Department of the Navy
Washington, DC 20362
Attn: S. M. Blazek
Code NSEA-05HB
(Copy No. 4)

Commander
Naval Sea Systems Command
Department of the Navy
Washington, DC 20362
Attn: A. R. Paladino
Code NSEA-05H1
(Copy No. 5)

Commander
Naval Sea Systems Command
Department of the Navy
Washington, DC 20362
Attn: F. B. Peterson
Code NSEA-052P
(Copy No. 6)

Commander
Naval Sea Systems Command
Department of the Navy
Washington, DC 20362
Attn: C. D. Smith
Code NSEA-63R
(Copy No. 7)

Commander
Naval Sea Systems Command
Department of the Navy
Washington, DC 20362
Attn: D. C. Houser
Code NSEA-63R14
(Copy No. 8)

Commander
Naval Sea Systems Command
Department of the Navy
Washington, DC 20362
Attn: F. J. Romano
Code NSEA-63R3
(Copy No. 9)

Commander
Naval Sea Systems Command
Department of the Navy
Washington, DC 20362
Attn: T. E. Peirce
Code NSEA-63R31
(Copy No. 10)

Commander
Naval Sea Systems Command
Department of the Navy
Washington, DC 20362
Attn: S. Silverstein
Code NSEA-63Y1
(Copy No. 11)

Commander
Naval Sea Systems Command
Department of the Navy
Washington, DC 20362
Attn: E. G. Liszka
Code PMS-406B
(Copy No. 12)

Commanding Officer
Naval Underwater Systems Center
Department of the Navy
Newport, RI 02840
Attn: T. A. Davis
Code 36314
(Copy No. 13)

DISTRIBUTION LIST FOR UNCLASSIFIED TECHNICAL MEMORANDUM FILE NO. 83-157, by G. C. Lauchle and G. B. Gurney, dated 9 September 1983 (continued)

Commanding Officer
Naval Underwater Systems Center
Department of the Navy
Newport, RI 02840
Attn: W. G. Fennel
Code 3634
(Copy No. 14)

Commanding Officer
Naval Underwater Systems Center
Department of the Navy
Newport, RI 02840
Attn: D. Goodrich
Code 3634
(Copy No. 15)

Commanding Officer
Naval Underwater Systems Center
Department of the Navy
Newport, RI 02840
Attn: C. Hervey
Code 3634
(Copy No. 16)

Commanding Officer
Naval Underwater Systems Center
Department of the Navy
Newport, RI 02840
Attn: R. H. Nadolink
Code 3634
(Copy No. 17)

Commanding Officer
Naval Underwater Systems Center
Department of the Navy
Newport, RI 02840
Attn: Library
Code 54
(Copy No. 18)

Commander
David W. Taylor Naval Ship
R&D Center
Department of the Navy
Bethesda, MD 20084
Attn: V. J. Monacella, Code 1504
(Copy No. 19)

Commander
David W. Taylor Naval Ship
R&D Center
Department of the Navy
Bethesda, MD 20084
Attn: Library, Code 1505
(Copy No. 20)

Commander
David W. Taylor Naval Ship
R&D Center
Department of the Navy
Bethesda, MD 20084
Attn: J. H. McCarthy, Code 154
(Copy No. 21)

Commander
David W. Taylor Naval Ship
R&D Center
Department of the Navy
Bethesda, MD 20084
Attn: P. Granville, Code 1541
(Copy No. 22)

Commander
David W. Taylor Naval Ship
R&D Center
Department of the Navy
Bethesda, MD 20084
Attn: T. T. Huang, Code 1552
(Copy No. 23)

Commander
David W. Taylor Naval Ship
R&D Center
Department of the Navy
Bethesda, MD 20084
Attn: M. M. Sevik, Code 19
(Copy No. 24)

Commander
David W. Taylor Naval Ship
R&D Center
Department of the Navy
Bethesda, MD 20084
Attn: W. K. Blake, Code 1905
(Copy No. 25)

DISTRIBUTION LIST FOR UNCLASSIFIED TECHNICAL MEMORANDUM FILE NO. 83-157, by G. C. Lauchle and G. B. Gurney, dated 9 September 1983 (continued)

Commander
David W. Taylor Naval Ship
R&D Center
Department of the Navy
Bethesda, MD 20084
Attn: R. A. Rippeon, Code 1908
(Copy No. 26)

Commander
David W. Taylor Naval Ship
R&D Center
Department of the Navy
Bethesda, MD 20084
Attn: F. S. Archibald, Code 1942
(Copy No. 27)

Commander
David W. Taylor Naval Ship
R&D Center
Department of the Navy
Bethesda, MD 20084
Attn: T. M. Farabee, Code 1942
(Copy No. 28)

Commander
David W. Taylor Naval Ship
R&D Center
Department of the Navy
Bethesda, MD 20084
Attn: F. E. Geib, 1942
(Copy No. 29)

Commanding Officer
Naval Undersea Warfare
Engineering Station
Department of the Navy
Keyport, WA 98345
Attn: Library
(Copy No. 30)

Commander
Naval Surface Weapons Center
Department of the Navy
Silver Spring, MD 20910
Attn: G. C. Gaunaurd
Code R-31
(Copy No. 31)

Commander
Naval Surface Weapons Center
Department of the Navy
Silver Spring, MD 20910
Attn: Library
(Copy No. 32)

Office of Naval Research
800 North Quincy Street
Department of the Navy
Arlington, VA 22217
Attn: M. M. Reischmann
Code 432F
(Copy No. 33)

Commanding Officer
Naval Ocean Systems Center
Department of the Navy
San Diego, CA 92152
Attn: E. W. Hendricks
Code 6342
(Copy No. 34)

Commanding Officer
Naval Ocean Systems Center
Department of the Navy
San Diego, CA 92152
Attn: D. M. Ladd
Code 6342
(Copy No. 35)

Commanding Officer
Naval Ocean Systems Center
Department of the Navy
San Diego, CA 92152
Attn: Library
(Copy No. 36)

Defense Technical Information
Center
5010 Duke Street
Cameron Station
Alexandria, VA 22314
(Copies 37 through 42)

DISTRIBUTION LIST FOR UNCLASSIFIED TECHNICAL MEMORANDUM FILE NO. 83-157, by G. C. Lauchle and G. B. Gurney, dated 9 September 1983 (continued)

Westinghouse Electric Corporation
Post Office Box 1488
Annapolis, MD 21404
Attn: Mr. R. Galino
(Copy No. 43)

Westinghouse Electric Corporation
Post Office Box 1488
Annapolis, MD 21404
Attn: Dr. R. F. Mons
(Copy No. 44)

Westinghouse Electric Corporation
Post Office Box 1488
Annapolis, MD 21404
Attn: Dr. G. W. Sjolander
(Copy No. 45)

NASA Langley Research Center
Hampton, VA 22665
Attn: Dr. D. Bushnell
(Copy No. 46)

Dr. R. J. Hansen
Naval Research Laboratory
Marine Technical Division
Washington, DC 20390
(Copy No. 47)

Mr. P. S. Klebanoff
National Bureau of Standards
Aerodynamics Section
Washington, DC 20234
(Copy No. 48)

Prof. D. G. Crighton
University of Leeds
Dept. Appl. Math. Studies
Leeds LS29JT
England
(Copy No. 49)

Dr. N. A. Brown
Bolt, Beranek and Newman
50 Moulton Street
Cambridge, MA 02136
(Copy No. 50)

Dr. K. L. Chandiramani
Bolt, Beranek and Newman
50 Moulton Street
Cambridge, MA 02136
(Copy No. 51)

Professor P. Leehey
Department of Ocean Engineering
Massachusetts Institute of Technology
77 Massachusetts Avenue
Cambridge, MA 02139
(Copy No. 52)

Professor J. L. Lumley
Sibley School of Mechanical and
Aeronautical Engineering
Upson Hall
Cornell University
Ithaca, NY 14850
(Copy No. 53)

Dr. R. E. A. Arndt
St. Anthony Falls Hydraulic Lab
University of Minnesota
Mississippi River at 3rd Ave., S.E.
Minneapolis, MN 55414
(Copy No. 54)

Professor V. J. Arakeri
Department of Mechanical Engineering
Indian Institute of Science
Bangalore 560 012
India
(Copy No. 55)

Dr. W. W. Haigh
Dynamics Technology, Inc.
22939 Hawthorne Blvd.
Suite 200
Torrance, CA 90503
(Copy No. 56)

DISTRIBUTION LIST FOR UNCLASSIFIED TECHNICAL MEMORANDUM FILE NO. 83-157, by G. C. Lauchle and G. B. Gurney, dated 9 September 1983 (continued)

Professor M. Pierucci
Department of Aerospace Engineering
and Engineering Mechanics
San Diego State University
San Diego, CA 92182
(Copy No. 57)

Dr. Carl Gazley, Jr.
Physical Science Department
The Rand Corporation
1700 Main Street
Santa Monica, CA 90406
(Copy No. 58)

Dr. W. S. King
Physical Science Department
The Rand Corporation
1700 Main Street
Santa Monica, CA 90406
(Copy No. 59)

Mr. Carl G. Jennings
Autonetics Division
Rockwell International Corp.
3370 Miraloma Avenue
Post Office Box 4921
Anaheim, CA 92803
(Copy No. 60)

Professor M. V. Morkovin
Dept. Mech. and Mechanical
and Aerospace Engineering
Illinois Institute of Technology
3300 S. Federal Street
Chicago, IL 60616
(Copy No. 61)

Professor Eli Reshotko
Case Western Reserve University
Cleveland, OH 44106
(Copy No. 62)

Professor C. L. Merkle
Department of Mechanical Engineering
The Pennsylvania State University
University Park, PA 16802
(Copy No. 63)

Director
Applied Research Laboratory
The Pennsylvania State University
Post Office Box 30
State College, PA 16801
Attn: S. Deutsch
(Copy No. 64)

Director
Applied Research Laboratory
The Pennsylvania State University
Post Office Box 30
State College, PA 16801
Attn: G. B. Gurney
(Copy No. 65)

Director
Applied Research Laboratory
The Pennsylvania State University
Post Office Box 30
State College, PA 16801
Attn: L. R. Hettche
(Copy No. 66)

Director
Applied Research Laboratory
The Pennsylvania State University
Post Office Box 30
State College, PA 16801
Attn: D. H. Kiely
(Copy No. 67)

Director
Applied Research Laboratory
The Pennsylvania State University
Post Office Box 30
State College, PA 16801
Attn: G. C. Lauchle
(Copy No. 68)

Director
Applied Research Laboratory
The Pennsylvania State University
Post Office Box 30
State College, PA 16801
Attn: B. R. Parkin
(Copy No. 69)

DISTRIBUTION LIST FOR UNCLASSIFIED TECHNICAL MEMORANDUM FILE NO. 83-157, by G. C. Lauchle and G. B. Gurney, dated 9 September 1983 (continued)

Director
Applied Research Laboratory
The Pennsylvania State University
Post Office Box 30
State College, PA 16801
Attn: Water Tunnel Files
(Copy No. 70)